Triptycene as a Supramolecular Additive in PTB7:PCBM blends and its Influence on Photovoltaic Properties

Lethy Krishnan Jagadamma[1], Liam J. McCarron[2], Alan A. Wiles[2], Victoria Savikhin[3, 4], Muhammad T. Sajjad[1], Mahdieh Yazdani[5], Vincent M Rotello[5], Michael F Toney[3], Graeme Cooke*[2], Ifor D. W. Samuel*[1]

[1]Organic Semiconductor Centre, SUPA, School of Physics and Astronomy, University of St. Andrews, St. Andrews, Fife, KY16 9SS, UK

[2]Glasgow Centre for Physical Organic Chemistry (GCPOC), WestCHEM, School of Chemistry, University of Glasgow, Glasgow, G12 8QQ, UK.

[3]Stanford Synchrotron Radiation Lightsource, SLAC National Accelerator Laboratory, 2575 Sand Hill Road, Menlo Park, CA 94025, United States

[4]Electrical Engineering Department, Stanford University, 350 Serra Mall, Stanford, CA 94305

[5]Department of Chemistry, University of Massachusetts Amherst, 710 North Pleasant Street, Amherst, Massachusetts 01003, United States

*E-mail: idws@st-andrews.ac.uk; Graeme.Cooke@glasgow.ac.uk

KEYWORDS: organic   solar   cells,   conjugated   polymer,   bulk   heterojunction, electroluminescence, phase separation

ABSTRACT: Additives play an important role in modifying the morphology and phase separation of donor and acceptor molecules in bulk heterojunction (BHJ) solar cells. Here we report triptycene (TPC) as a small molecule additive for supramolecular control of phase separation and concomitant improvement of the power conversion efficiency (PCE) of PTB7 donor and fullerene acceptor based BHJ polymer solar cells. An overall 60% improvement in PCE is observed for both PTB7:$PC_{61}BM$ and PTB7:$PC_{71}BM$ blends. The improved PV performance can be attributed to three factors: (a) TPC induced supramolecular interactions with donor:acceptor components in the blends to realise a nanoscale phase separated morphology (b) an increase in the charge transfer (CT) state energy that lowers the driving force for electron transfer from donor to acceptor molecules; and (c) an increase in the charge carrier mobility. An improvement in efficiency using TPC as a supramolecular additive has also been demonstrated for other BHJ blends such as PBDB-T:$PC_{71}BM$ and P3HT:PCBM implying the wide applicability of this new additive molecule. A comparison of the photostability of TPC as an additive for PTB7:PCBM solar cells to that of the widely used 1,8- diiodooctane (DIO) additive shows ~ 30 % higher retention of photovoltaic performance for the TPC-added solar cells after 34 hours of AM 1.5G illumination. The results obtained suggest that the approach of using additives that can promote supramolecular interactions to modify the length scale of phase separation between donor and acceptor is very promising and can lead to the development of highly efficient and stable organic photovoltaics.

1. INTRODUCTION

Among the third- generation thin film photovoltaics, organic solar cells are especially attractive due to their low cost, high throughput processability and environmentally friendly energy conversion. Lab scale organic solar cells have recently achieved significant advances in

device performance, with 12% power conversion efficiency (PCE).[1-2] This improvement has been realized by breakthroughs in material development, interface engineering, some control of morphology, and processing conditions of the organic active layer. Since the conjugated organic semiconductors are limited by low exciton diffusion length (10-20 nm) in comparison to their absorption length (few hundred nanometers), morphological control of the organic solar cell active layer is crucial in achieving high power conversion efficiency.[3-4] The large-scale phase separation of donor and acceptor molecules to their own pure phase domains with sizes of tens and hundreds of nanometers leads to geminate recombination of the photogenerated singlet exciton. Moreover, a discontinuous morphology with very fine mixing can result in inefficient transport and increases the probability of non-geminate recombination of photogenerated charge carriers.[5-6] To obtain high performance organic solar cells, the morphology of the donor:acceptor blend should be such that there is a balance between nanoscale phase separation of the blend components and bi-continuous percolative pathways to the charge collecting electrodes.

Enhanced bulk heterojunction morphology can be obtained by adopting processing methodologies such as thermal annealing[7-8], solvent vapour annealing[9-10] and using solvent additives.[11] Among these, the most widely accepted and effective approach that is compatible with large scale processing is that of using high boiling point solvent additives. The most commonly used solvent additive in BHJs consisting of low-bandgap polymers such as PTB7 and PTB7-Th is 1,8-diiodooctane (DIO), and has enabled high PCEs to be achieved by selectively dissolving the PCBM aggregates and homogeneously mixing the donor polymer with the fullerene acceptor resulting in a nanoscale intermixed morphology. [12] Despite the advantage of DIO in enhancing the PCE, recently it has been reported that residual DIO (because of high boiling point of 333 ^{o}C and low vapour pressure of 0.037 Pa at room temperature)[13] in the active

layer blend dramatically decreases the photostability of the PTB7-Th donor and accelerates the chemical degradation of PTB7-Th:PC$_{71}$BM blend upon exposure to air and light.[14-15] Lee et al[16] also observed that the iodine in residual DIO functions as trap centres that impede charge transport and mediate the oxidation of fullerene. Jacobs et al[17] have recently shown that DIO impurity still exists in the organic active layer blend even after the blend film had undergone sequential heating and vacuum evaporation steps to remove DIO. Hence the development of an iodine-free additive molecule that enhances the power conversion efficiency of the low-bandgap polymer: acceptor system is very important for the further development of efficient and stable organic photovoltaics.

Additive-assisted nanoscale morphology, in most cases, enhances the power conversion efficiency by improving the short circuit current density (J$_{sc}$) and fill factor (FF) due to increased D-A interfacial area and percolation pathways. One of the factors that limits the efficiency of organic solar cells, is the high loss of open circuit voltage (V$_{oc}$) compared to the gap between the HOMO of the donor and LUMO of the acceptor. This is partly due to the low LUMO level of fullerene molecules, which increases the charge transfer loss due to vibrational relaxation.[18] Moreover, functionalization of fullerene molecules to raise the LUMO level is difficult.[19] Tailoring the bulk heterojunction morphology and relating these morphological features to V$_{oc}$ is still an open challenge in organic solar cells and previous reports imply that modification in donor-acceptor morphologies does not necessarily yield improvement in V$_{oc}$.[20-21] However, to pursue the maximum PCE of OPVs, this bottleneck of low photovoltage in comparison to donor-acceptor HOMO-LUMO gap should be overcome. Hence strategies to improve the V$_{oc}$, for a selected donor-acceptor system, are crucial as they can provide the basis of a new design rule for realizing more efficient organic solar cells.

An important issue in solution processing of bulk hetero-junction solar cell devices is how the donor and acceptor molecules pack together in the blend film which in turn can influence the processes of photogeneration of charges, their transport and hence the overall power conversion efficiency. Here we explore the approach of controlling aggregation *via* supramolecular interactions to beneficially modify the length scale of phase separation between the donor and acceptor molecules and their HOMO-LUMO gap in the BHJ blend. The use of triptycene (TPC) as a new class of additive for promoting this type of supramolecular interactions is demonstrated for three different BHJ blends. The TPC interacts and influences the solid-state organization of fullerene molecules, and improves the photovoltaic properties of PTB7:$PC_{61}BM$ and PTB7:$PC_{71}BM$ BHJ blends. Triptycene is a simple and readily available molecule which has been explored for a variety of supramolecular host-guest interactions.[22-23] It is composed of a benzene functionalized bicyclo[2.2.2]octane ring. Its bicyclic core confers a rigid three-dimensional paddle wheel structure **[Figure 1a]** with three open electron-rich cavities which have been shown to bind fullerene molecules.[22-25] The potential of TPC to template the macroscopic assembly of fullerene molecules in neat films and within a polymer-fullerene blend film and thereby control the phase separation has been previously reported for C_{60} and MEH-PPV:C_{60} blends.[26-28] However, no improvement in photovoltaic properties of BHJ blends due to addition of non-functionalised TPC has been reported so far.

In the present work, we demonstrate TPC as an efficient additive molecule to enhance the photovoltaic power conversion efficiency of PTB7:PCBM blends by 60% by utilizing their property to promote supramolecular self-assembly. We find that the addition of an optimum amount of TPC not only enhances the FF and J_{sc} of the respective organic solar cells but also results in an increase of V_{oc} by 40-50 meV. We attribute the origin of the improved V_{oc} to the

higher charge transfer (CT) state energy of PTB7:PCBM blends in which TPC has been added. This is substantiated by the corresponding electroluminescence spectra and reduced electron affinity of fullerene molecules with added TPC. We observe that the optimum amount of TPC to maximize the photovoltaic performance largely depends on the symmetry of the fullerene molecule in the blend. Overall, TPC enhances the PTB7:PCBM BHJ solar cell efficiency *via* (a) modifying the nano-scale morphology of the donor: acceptor blend, (b) increasing the charge transfer state energy and the V_{oc} and (c) improving the mobility of charge carriers. Apart from the PTB7:PCBM blend, the applicability of TPC as an additive has been successfully demonstrated for other BHJs such as PBDB-T:PC_{71}BM and P3HT:PCBM. Further, improved photostability (~ 30 % better) is demonstrated for PTB7:PCBM blend systems with TPC added in comparison to PTB7:PCBM blend added with DIO. This novel concept of using TPC as an additive to improve the OPV performance using supramolecular interactions has the potential to be used in other organic optoelectronic devices as well. In the following sections, influence of TPC onto the photovoltaic properties of PTB7:PC_{61}BM, PTB7:PC_{71}BM blends and the various optoelectronic and microstructural changes due to supramolecular interactions induced by TPC and its implication in photovoltaic properties are discussed.

2. EXPERIMENTAL DETAILS:

2.1 Fabrication of PTB7:PCBM blend inverted solar cells

Inverted organic solar cells were fabricated on pre-patterned ITO-coated glass. The ITO-coated glass substrates were cleaned in detergent (sodium dodecyl sulphate-SDS), successively ultrasonicated in deionized water, acetone, and isopropyl alcohol, and exposed to Plasma Asher for 3 minutes. The PTB7:PC_{61}BM and PTB7:PC_{71}BM blend solutions were prepared by dissolving the components in a ratio of 1:1.5 (by weight), with a total concentration of 25 mg/mL

in chlorobenzene, with 3 vol% DIO. The solution was kept stirring at 60°C for ~8 h before spin-coating. TPC solutions were prepared at concentrations of 1, 3, 5, 10, 50, 100, 250 mg/mL in chlorobenzene and stirred at 60 °C for at least 2 hours. To find the optimum concentration of TPC for these BHJ blends, 5 vol% of TPC solution was added and solutions were stirred for an additional 3 hours at 60 °C. This resulted in overall TPC concentrations of 0.05, 0.15, 0.25, 0.5, 2.5, 5, and 12.5 mg/mL respectively. The control (no TPC) sample was prepared by adding an equal amount of chlorobenzene solvent to the respective blend solution. In the case of P3HT:PCBM and PBDB-T:PCBM, blend solutions were prepared by mixing 1:1 (wt%) donor to acceptor with a total concentration of 50 and 20 mg/mL in o-dichlorobenzene (oDCB). In all the inverted organic solar cells fabricated, the electron transporting layer was amorphous ZnO (a-ZnO) thin film having thickness ~ 25 nm and was prepared according to a previous report.[29] The precursor solution for ZnO was prepared by dissolving equimolar (0.11 M) ratio of zinc acetate dihydrate (ZAD) [$Zn(CH_3COO)_2.2H_2O$, Sigma Aldrich 99.9%] and monoethanol amine (MEA) ($NH_2CH_2CH_2OH$) in 2-methoxy ethanol ($CH_3OCH_2CH_2OH$), Sigma Aldrich 99.8%). The precursor solution was continuously stirred at room temperature for ~24 hours before spin coating onto the cleaned ITO substrate. The spin speed was 2000 rpm for 30 seconds and after spin coating the films were annealed in air at 125 °C for 10 minutes. The active layer was deposited by spin - coating (1000 rpm, 60 s) on glass/ITO/a-ZnO substrates inside a nitrogen filled glove box. The samples were then transferred to a vacuum thermal evaporator (1 x10^{-6} mbar base pressure) and kept under vacuum overnight before thermally evaporating the hole transporting layer of MoO_x (7 nm) and anode Ag (100 nm) using a shadow mask. The active area of the device was 0.07 cm^2. All the processing related to the active layer was performed inside a nitrogen-filled glove box.

After the electrode deposition, the devices were encapsulated with a UV optical adhesive and a glass coverslip. The current–voltage characteristics were determined under an illumination intensity of 100 mW/cm^2 in air using an air mass 1.5 global (AM 1.5G) Sciencetech solar simulator and a Keithley 2400 source-measure unit. The illumination intensity was verified with a calibrated monosilicon detector and a KG-5 filter. The external quantum efficiency (EQE) measurements were performed at zero bias by illuminating the device with monochromatic light supplied from a Xenon arc lamp in combination with a dual-grating monochromator. The number of photons incident on the sample was calculated for each wavelength by using a silicon photodiode calibrated by national physical laboratory (NPL).

2.2 Characterization of TPC and PTB7:PCBM active layer blend

The surface morphology of the PTB7:PC$_{71}$BM films was characterized using atomic force microscopy (AFM). AFM images were obtained with a Bruker MultiMode 8 instrument in the tapping mode. NANOSENSORS™ PPP-NCSTR Si cantilever tips with force constant of 6–7 Nm^{-1} were used as AFM probes. Steady state absorption spectra of the blend films were recorded using a Cary 300 spectrometer for the wavelength range of 300-800 nm. For this, the active layer blend was deposited under identical conditions to that used for OPV devices on a quartz disc. The thickness of the active layer blend is measured using Dektak II profilometer (stylus force 6 mg and a measurement range of 6.5 μm). The thickness of the PTB7:PC$_{61}$BM blends with and without TPC added are respectively 106 and 117 nm and for PTB7:PC$_{71}$BM blends these values are 123 and 135 nm respectively. Steady state PL spectra were measured with a Hamamatsu streak camera C10910-05 with S-20ER photocathode and 650 nm as excitation wavelength from an optical parametric amplifier pumped by Pharos laser (from Light Conversion).

Grazing Incidence Wide-Angle X-Ray Scattering (GIWAXS) experiments were performed at Stanford Synchrotron Radiation Lightsource (SSRL) beamline 11-3, with an incident energy of 12.735 keV and a MARCCD detector at a sample-detector distance of 250 mm. For these experiments, blends were spin-coated directly onto cleaned Silicon using procedures outlined above. An incident angle of 0.14° was used and five 60-second exposures were averaged. Data was calibrated (LaB$_6$ calibrant at 3° incident angle), dezingered, and averaged in Nika software[30] and geometry corrections were performed using WAXStools software.[31] Additional integration and correction was done using custom written scripts. Data was corrected by the Monitor value (corresponding to beam intensity) and film thickness. Length correction was not used as all samples in each set had approximately the same dimensions.

We applied custom peak fitting to extract quantitative information from GIWAXS images. The first fitting was for Q=0.31 to 1.01 Å^{-1} and included three Gaussian peaks on a linear background: two for the first and third order PTB7 alkyl peaks and one for the PCBM peak at 0.7 Å^{-1}. The second fitting was for Q=1.1 to 2.75 Å^{-1} and included three Gaussians on a linear background: the PTB7 π-π stacking peak and two PCBM peaks. Fitting was performed to each 10° cake slice to extract pole figures. The pole figures were interpolated into the inaccessible out-of-plane region using MATLAB's spline function. The geometric sin(angle) correction was applied before integrating the pole figures to get total peak volume (related to degree of crystallinity). While this method reliably extracted peak intensities, peak positions were somewhat inaccurate due to asymmetric peak shapes and overlap. For this reason we report a visual estimate of peak position from a circular integration in Table S9.

To calculate thickness for GIWAXS normalization, we used a Bruker Dektak 150 using 1 mg stylus force or a Bruker Dektak XT using 0.1 mg stylus force (6.5 μm measurement range for

both). Consecutive scans at the same location were compared to ensure that the stylus was not scratching the film surface. A razor was used to scratch lines of film off the Silicon substrate in three places: in the middle of the sample and on each of two edges. A weighted average was taken of thickness measurements from the three positions to better represent the average irradiated thickness.

HOMO levels of the $PC_{61}BM$, $PC_{71}BM$, PTB7 films with and without TPC were measured using UV-Air Photoemission Systems (KP Technology APS03 instrument). The Kelvin probe tip has a gold-alloy coating (2 mm diameter) and when used in contact potential difference (CPD) mode vibrates at 70 Hz at an average height of 1 mm from the sample surface. For recording the ambient photoemission spectrum (APS), the sample was illuminated with a 4-5 mm diameter light spot from a tunable monochromated D_2 lamp (4–7 eV). The raw photoemission data were corrected for detector offset; intensity normalised then processed by a cube root power law. The energy resolution in APS mode is 50-100 meV.

The electron and hole mobility of the PTB7:PCBM blends with and without TPC added were measured using space charge limited current (SCLC) method. For this the active layer was prepared under the same conditions as for the corresponding organic solar cells. The hole-only devices consisted of glass/ITO/PEDOT:PSS/active layer/MoO_3(10 nm)/Ag and the electron-only devices consisted of glass/Al (80 nm)/active layer/LiF (1 nm)/Al (80 nm).

The UV-vis spectra of the TPC solution was recorded on a Perkin-Elmer Lamda 25 instrument. The solution was prepared using anhydrous CH_2Cl_2 at 1×10^{-5} M. The interaction of triptycene with $PC_{61}BM$ in the solution state was examined using fluorescence quenching studies. Using a fluorescence microplate reader (Molecular Devices Spectra Max M2), the change in emission spectra of a 0.04 mg/mL TPC solution was recorded upon injection

of different concentrations of $PC_{61}BM$. All measurements were performed in chlorobenzene (using a quartz cuvette) to mimic the spin-coating conditions. The excitation wavelength used was 310 nm. Cyclic and square wave voltammetry measurements were carried out using a CH Instruments 440a electrochemical analyser. Solution electrochemistry was performed using a platinum working electrode, a platinum wire counter electrode and a silver wire pseudo-reference electrode. Ferrocene was used as an internal standard, with the ferrocene/ferrocenium (Fc/F+) redox couple adjusted to 0.0 V. The solutions were prepared using anhydrous CH_2Cl_2 containing 1×10^{-3} M triptycene, electrochemical grade tetrabutylammonium hexafluorophosphate (0.1 M) as the supporting electrolyte. The solutions were purged with nitrogen gas for 3 minutes prior to recording the electrochemical data. Solid-state voltammetry was performed using sputtered ITO (15 Ω/sq.) thin films on glass slides (2 cm $\times$ 2 cm) as the working electrode, a platinum wire counter electrode and a saturated silver/silver chloride reference electrode, immersed in a potassium chloride buffer solution as the electrolyte (3 M). The thin films were prepared using the same protocol as reported above for the device fabrication. The electrolyte was degassed with nitrogen for 3 minutes prior to recording the data. NMR spectra was obtained with a Bruker AVIII 400 MHz spectrometer and chemical shifts are relative to trimethylsilane. Gaussian 09 [32] was used to estimate the HOMO and LUMO levels of triptycene. The geometry of triptycene was initially optimised semi-empirically (PM6) and then re-optimised at DFT (B3LYP/6-31G*). The resulting structures were local minima, as none of the vibrational frequencies generated imaginary frequencies.

2. RESULTS AND DISCUSSION:

2.1 Effect of TPC on the photovoltaic properties of PTB7:PC_{61}BM blends

To investigate the effect of TPC on the photovoltaic properties of the PTB7-PC$_{61}$BM blend, TPC in chlorobenzene was prepared for a range of concentrations and is mixed with the active layer blend as described in the experimental section. The molecular structures of the donor and acceptor molecules are shown in **Figure 1(b)-(d)** and the OPV device architecture is shown in Figure in 1(e). J-V characteristics of the PTB7:PC$_{61}$BM devices with and without TPC are shown in **Figure 2(a)** and photovoltaic performance parameters as a function of TPC concentration are plotted in **Figure 2(b)** (and listed in Table S1). These plots show that, with increase in concentration of TPC, the photovoltaic parameters V_{oc} and FF gradually increase, and maximum PCE of 5.7% is observed for TPC concentration of 7.5 mg/mL (corresponding to a molar ratio of ~1:2 for PC$_{61}$BM:TPC), compared with a PCE of 3.5% for control devices without TPC. Thus, under the optimum conditions of TPC addition, the PCE is increased by ~ 60%. The open circuit voltage increased from 0.75 V to 0.79 V (increase of ~ 7%), and the highest improvement is seen in fill factor from 39% to 58% (increase by ~ 50 %) with J_{sc} showing improvement of ~ 5%. The presence of TPC in the completed solar cell devices was confirmed by ^{1}H NMR spectra of the re-dissolved blends shown in Figure S1. The ratio of amount of PC$_{61}$BM fullerene to TPC obtained from integrating the NMR spectra was 1:1.03.
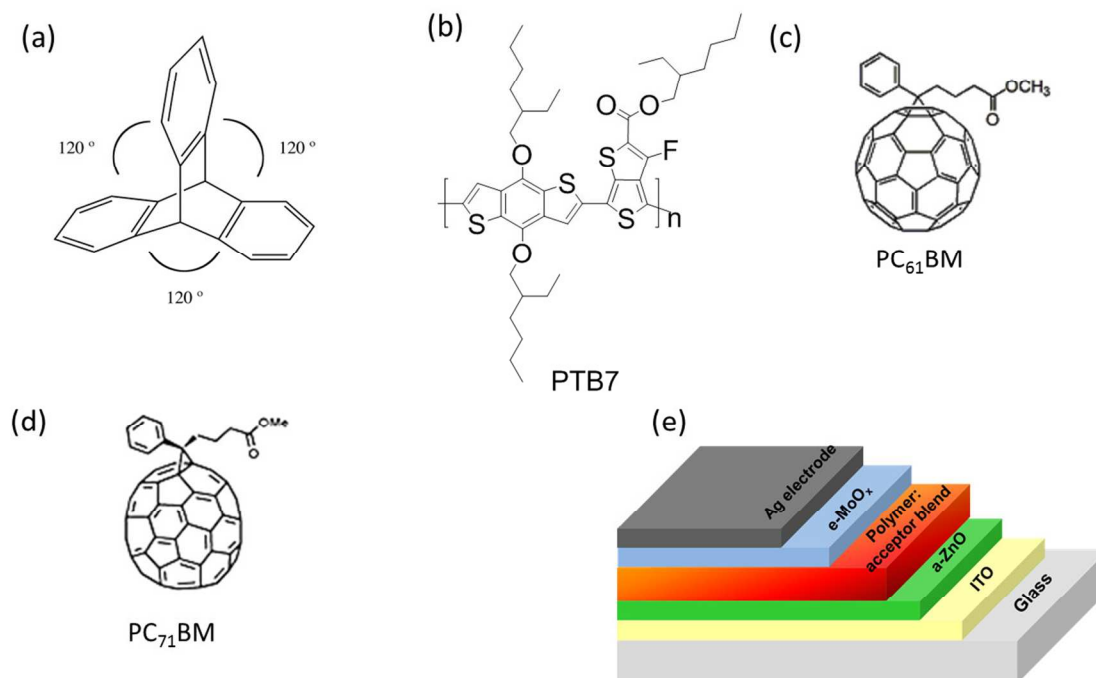
Figure 1. Molecular structure of (a) triptycene (TPC) (b) PTB7 (c) $PC_{61}BM$ and (d) $PC_{71}BM$ (e) device architecture used for solar cell fabrication.

For comparison, the influence of DIO was studied by fabricating PTB7:PC_{61}BM devices with and without DIO additive (**Figure S2** and **Table S2**). In the presence of DIO as a solvent additive, the PCE of the OPV devices almost doubles, primarily due to an enhancement in fill factor and short circuit current density. This increase in PCE with DIO as an additive is consistent with previous reports where the influence of DIO on the photovoltaic properties of PTB7:PCBM blend has been studied extensively.[6, 33-34] The DIO effect has mostly been attributed to the optimization of the phase-separated nano-scale morphology of polymer:fullerene blend. Recent charge carrier dynamic studies have shown that DIO as a solvent additive increases the charge generation rate, reduces geminate and bimolecular recombination, and increases the electron mobility.[6, 35] Even though the power conversion efficiency of

PTB7:PC$_{61}$BM blend with TPC as additive is lower than that due to DIO additive, the overall improvement of PCE for PTB7:PC$_{61}$BM blend with TPC addition is interesting, particularly the V$_{oc}$ increase of ~ 40 -50 mV which is not reported in previous works of functionalized TPC.[36-37] The EQE spectra of the PTB7:PC$_{61}$BM devices with and without TPC under optimum conditions are shown in **Figure 2(c)**. Since the J$_{sc}$ increases by only a small amount with the introduction of TPC, EQE data only shows a slight overall increase. The J$_{sc}$ values obtained by integrating the EQE spectra are also shown in Figure 2(c). The calculated integrated current density values from the EQE spectra are 10.5 and 11 mA/cm^2 for PTB7:PC$_{61}$BM and TPC:PTB7:PC$_{61}$BM solar cells and are close to the measured J$_{sc}$ values as listed in Table S1. To investigate the combined effect of TPC and DIO as additives in improving the PCE of PTB7: PC$_{61}$BM blends, solar cells were fabricated using the optimised conditions of these two additives (**Table S3** and **Figure S3)**. Even though the PCEs of the devices with two additives are better than those of the devices containing TPC alone, the overall PCE is highest for PTB7:PC$_{61}$BM blends added with DIO.
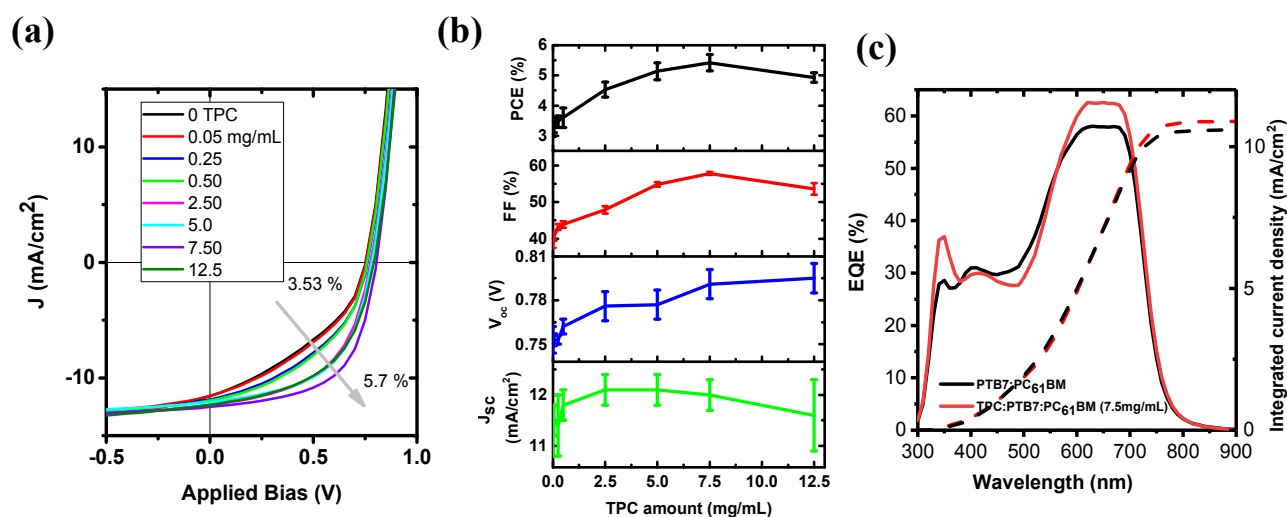
Figure 2. (a) J-V characteristics and (b) photovoltaic performance parameters of the PTB7:PC$_{61}$BM blends as a function of different TPC contents (c) EQE spectra and the corresponding integrated current density of the control and the PTB7:PC$_{61}$BM bulk heterojunction solar cells added with optimum TPC content.

2.2 Effect of TPC on the photovoltaic properties of PTB7:PC$_{71}$BM blends

To investigate how the symmetry of the fullerene acceptor molecule affects the photovoltaic properties of blends added with TPC, solar cells were fabricated using PTB7:PC$_{71}$BM blends with TPC as additive. The TPC was added to the PTB7:PC$_{71}$BM blends similarly to the optimized procedures for PTB7:PC$_{61}$BM blend. **Figure 3(a) and (b)** show the J-V characteristics and the corresponding photovoltaic properties as a function of TPC concentration in the blend. The photovoltaic performance parameters are listed in **Table S4**. In contrast to PTB7:PC$_{61}$BM blend, where 7.5 mg/mL is optimum for the best PCE, performance continues to improve through 12.5 mg/mL in the PTB7:PC$_{71}$BM blend (corresponding to a molar ratio of ~1:3 for PC$_{71}$BM:TPC). [The ratio of the PC$_{71}$BM fullerene to TPC estimated from integrating the NMR spectra was 1:1.53]. With the addition of 12.5 mg/mL TPC, the PCE improves by ~60% from 2.33% to 3.76%. The improvements in photovoltaic performance

parameters are 33.5% in J_{sc}, 16.6% in FF, and 4.6% in V_{oc}. The EQE spectra and the corresponding integrated current density of the PTB7:PC$_{71}$BM devices with and without TPC under optimum conditions are shown in **Figure 3(c)**. The enhancement in EQE with the TPC addition is well matching with the improvement in J_{sc} as shown in **Figure 3(a) and (b)**. The integrated current density values obtained from the EQE spectra are 7.9 and 12.3 mA/cm^2 for PTB7:PC$_{71}$BM solar cells with and without TPC under optimum conditions and are close to the experimentally measured J_{sc} values listed in Table S4. To explain this improvement in J_{sc}, the dependence of photocurrent density (J_{ph}) on the effective voltage (V_{eff}) was measured for PTB7:PC$_{71}$BM solar cells with and without TPC added [Figure S4 (a)]. Higher photocurrent density was observed for PTB7:PC$_{71}$BM solar cells with TPC added. The exciton dissociation probability $P(E,T)$ at any applied bias is obtained from the plot of normalised photocurrent density with respect to the effective voltage [Figure S4 (b)]. The dissociation probability value estimated from this plot were 47 % for devices without TPC and 55 % for devices with TPC.
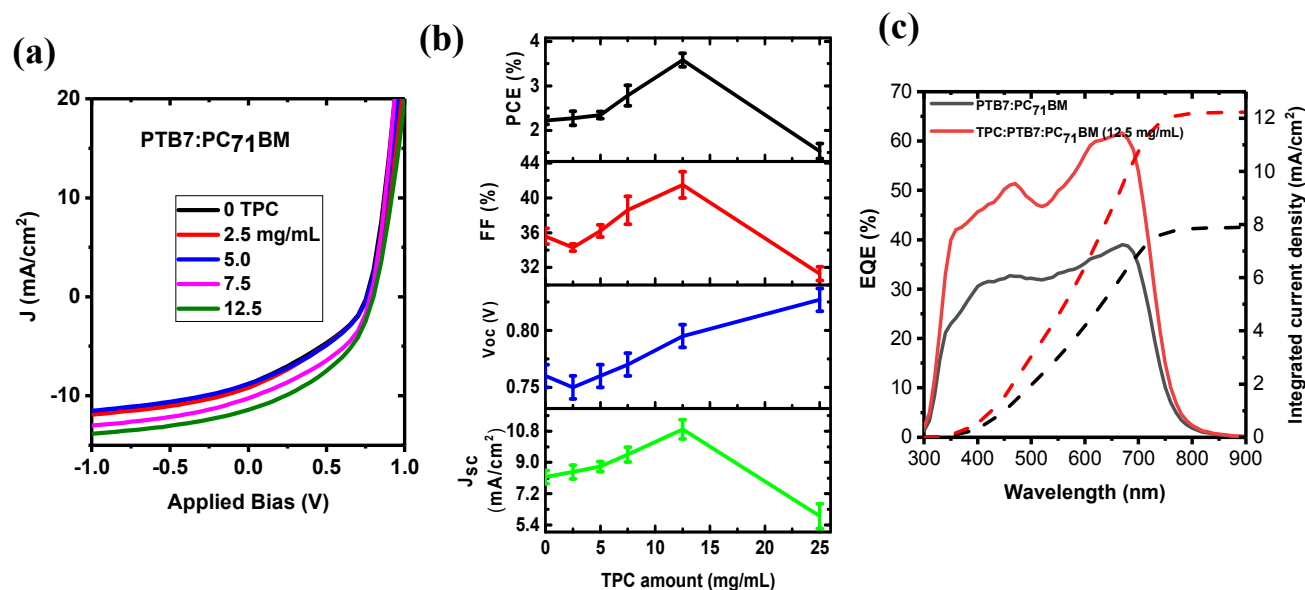
Figure 3(a) J-V characteristics and (b) the photovoltaic performance parameters of the PTB7:$PC_{71}BM$ blends as a function of different TPC incorporation (c) EQE spectra and the corresponding integrated current density of the control and the PTB7:$PC_{71}BM$ bulk heterojunction solar cells added with optimum TPC content (12.5 mg/mL).

To compare the effect of TPC additive to the DIO additive, reference devices were prepared based on PTB7:$PC_{71}BM$ blends with and without DIO (**Figure S5** and **Table S5)**. Similar to PTB7:$PC_{61}BM$ blend, the power conversion efficiency dramatically increases from 2.33 to 7.81% due to the addition of DIO. The PCE almost triples with the addition of DIO, the main difference being in the FF (35 vs 71%) and short circuit current density (8.85 to 15.2 mA/cm^2). The improvement in PCE for PTB7:$PC_{71}BM$ blend solar cells due to DIO is also reported to be due to the optimized phase-separated nano-morphology of polymer:fullerene blends and reducing the recombination losses.[6, 38-39]

A comparison of the influence of DIO and TPC as additives to the BHJ blends of PTB7:$PC_{61}BM$ and PTB7:$PC_{71}BM$ reveals different behaviour in the enhancement of photovoltaic performance properties. In the case of DIO additive, the improvement is mainly obtained for FF and J_{sc} and is the same for both blend systems irrespective of the fullerene molecule in the blend. However, when TPC is incorporated as an additive, the blends of PTB7:$PC_{61}BM$ and PTB7:$PC_{71}BM$ have different photovoltaic response in terms of their performance parameters, especially in their FF and J_{sc}. The PV performance parameter which exhibited the highest enhancement (~50 %) is FF for PTB7:$PC_{61}BM$ blend and in J_{sc} (~35%) for PTB7:$PC_{71}BM$ blend. Moreover, the experimentally obtained molar ratio of TPC to fullerene molecules corresponding to highest photovoltaic performance, is different for PTB7:$PC_{61}BM$ and PTB7:$PC_{71}BM$ blends: ~2:1 *vs* over 3:1 respectively. This suggests a relationship between

the TPC additive in the blend and the symmetry of the fullerene acceptor molecule, since in both blend systems the donor molecule is PTB7. As previously reported, the main difference between $PC_{61}BM$ and $PC_{71}BM$ is the ellipsoidal symmetry of the latter and the spherical symmetry of the former.[40] Considering the fullerene moiety alone, the aspect ratio (ratio of height to width) is respectively 1:1 and 1:1.14, whereas by including the methano-bridge carbon as well, the aspect ratio is respectively 1:1.19 and 1:1.33. Because of this difference in symmetry of the fullerene molecules in the blend, the concave arrangement of the three phenyl moieties in the TPC molecule may be interacting differently with $PC_{61}BM$ and $PC_{71}BM$ resulting in dissimilar molecular packing effect and intermolecular electronic coupling.[41] Since in PTB7:$PC_{61}BM$ blends, the optimized molar ratio of $PC_{61}BM$:TPC is ~1:2, this may suggest TPC molecules are interacting with the fullerenes to form two-component extended structures, through π-π supramolecular interactions with each $PC_{61}BM$ molecule being surrounded by two TPC molecules. This is consistent with the packing observed in the case of the C_{60}:TPC co-crystal.[41] However, for PTB7:$PC_{71}BM$ blend, the optimum OPV performance corresponds to a molar ratio of $PC_{71}BM$: TPC at ~1:3, and following the same argument as in the case of C_{60} : TPC co-crystal, this would imply that each $PC_{71}BM$ is surrounded by an average of three TPC molecules. These different optimum ratios of fullerene:TPC in $PC_{71}BM$ and $PC_{61}BM$ imply the possibility of different supramolecular interactions triggered by TPC molecules in their blends with PTB7. In addition to the effect of TPC on the supramolecular interaction with that of fullerene molecules, there is also an effect on PTB7 as can be seen from the blue shift in the absorption edge and an increase in the alkyl spacing as discussed in sections 2.4 and 2.5(b).

2.3. Recombination mechanisms of PTB7:$PC_{61}BM$ devices
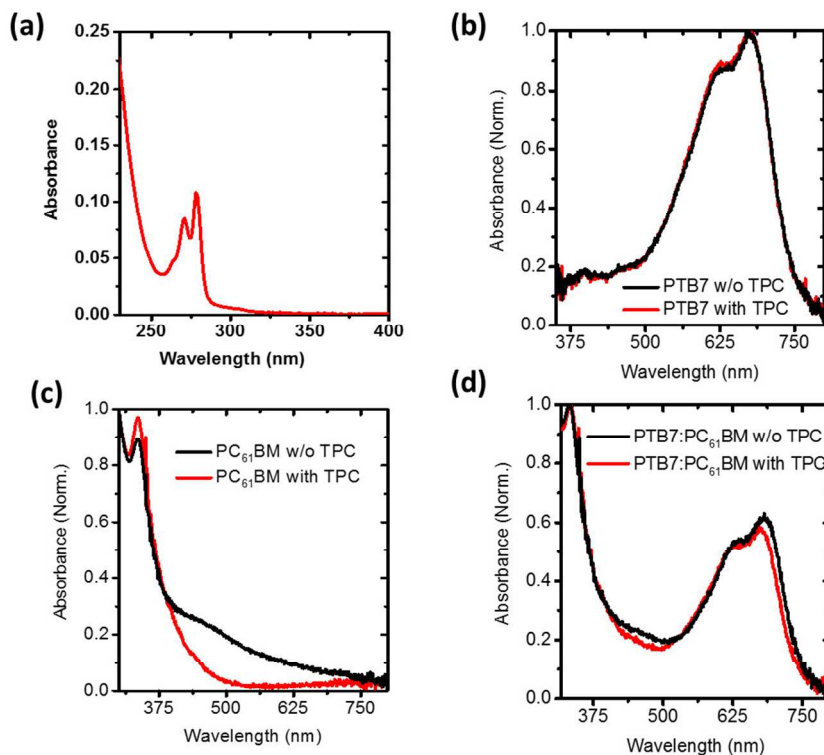
To understand why the TPC incorporation improves the photovoltaic properties of PTB7:PC$_{61}$BM blend, the recombination mechanisms in the solar cells were studied using light intensity dependence of J-V characteristics (**Figure S6**). A detailed discussion is given in SI. No significant differences were observed in the dependence of both V$_{oc}$ and J$_{sc}$ on incident light intensity for PTB7:PC$_{61}$BM blends with and without TPC content. Thus, since the studies on recombination mechanisms show only marginal differences, which cannot account for the improved photovoltaic properties upon the TPC incorporation, detailed optical and microstructural characterizations were performed as described below. In all the characterizations below, neat or blend films added with TPC imply use of the best performing content of TPC as previously determined (7.5 mg/mL or 12.5 mg/mL for PTB7:PC$_{61}$BM and PTB7:PC$_{71}$BM blends respectively).

2.4. Optoelectronic properties of the PTB7:PC$_{61}$BM blends

UV-VIS absorption spectra of the TPC molecules in solution and thin films of PTB7, PC$_{61}$BM and the blend PTB7:PC$_{61}$BM with and without TPC are shown in **Figure 4 (a)-(d)**. The absorption spectra of TPC molecules is mainly in the deep UV region and hence does not contribute towards the absorption of the active layer of the solar cells. With the addition of TPC molecules into PTB7, no spectral shift is observed and the overall absorption spectral features remains the same. Similar observation in absorption features has been previously reported for MEH-PPV films added with TPC.[26] On the other hand, the absorption profile of PC$_{61}$BM changes significantly when TPC is added. The absorption intensity at 420-500 nm wavelength range is considerably reduced for the films containing TPC compared to the neat PC$_{61}$BM films. A similar observation has been previously reported by Konarev *et al.*[27] for single crystals of C$_{60}$ versus the TPC:C$_{60}$ co-crystal. The absorption in the wavelength range of 420-500 nm has been

attributed to the intermolecular HOMO-LUMO transitions between adjacent fullerene molecules.[42] The lowered intensity of this absorption band shows that TPC incorporation alters the local environment of $PC_{61}BM$ molecules by a possible supramolecular assembly of $PC_{61}BM$ with TPC molecules as reported by Veen *et al.*[28] and hence modifies the intermolecular interactions of $PC_{61}BM$ molecules between themselves.[43] To confirm this potential supramolecular assembly process, fluorescence quenching studies were performed. Triptycene is a highly fluorescent material. The emission spectra of TPC solution (0.04 mg/mL) in chlorobenzene and the quenching of this fluorescence due to different concentrations of $PC_{61}BM$ incorporation are shown in **Figure S7(a) & (b)**. Substantial (~50%) quenching is observed using a solution of ~ 0.04 mg/mL (~ 0.15 mM) TPC and ~ 6.6×10^{-5} mg/mL (~7.2×10^{-5} mM) $PC_{61}BM$. This strong fluorescence quenching by a very small amount of fullerene (fullerene to triptycene ratio~ 1:2100) implies strong supramolecular assembly (guest-host complex formation) triggered

by $PC_{61}BM$ is occurring prior to the spin-coating process itself.[44] Since the strength of the PL

quenching (~50 %) of TPC by a small amount of PCBM is surprising, the experiment was

Figure 4. The UV-VIS absorption spectra of (a) TPC molecules in solution 1×10^{-5} M in DCM,

(b) PTB7&PTB7:TPC (c) $PC_{61}BM$ & $PC_{61}BM$:TPC, and (d) PTB7:$PC_{61}BM$& B7:$PC_{61}BM$:TPC

thin films.

repeated and the same result obtained. To understand how this strong interaction between TPC

and $PC_{61}BM$ affects thin film formation, PL emission spectra of $PC_{61}BM$ films with and without

TPC were recorded as shown in Figure S8 (a).

Even though the overall spectral shape remains the same, the PL emission from

$PC_{61}BM$:TPC films is blue-shifted and with narrower FWHM compared to emission from neat

$PC_{61}BM$. This observed spectral feature is similar to what Lomas *et al.*[26] have previously

reported for C_{60} and TPC:C_{60} co-crystals. The observed spectral shift due to TPC incorporation indicates TPC increases the separation between the $PC_{61}BM$ molecules (in agreement with UV-vis absorption spectra in Figure 4(c) and prevents the formation of energetically stabilized delocalized aggregate states in $PC_{61}BM$ films.[26] However no significant differences in PL emission spectra were observed [Figure S8(b)] for the PTB7 donor molecules added with TPC in comparison to neat PTB7 films and this is similar to the previously reported behaviour for MEH-PPV donor polymers added with TPC.[26]

The absorption spectra of the blend films [Figure 4(d)] can be considered as an overlap of the spectral features of TPC added donor and acceptor. The decrease in absorption intensity in the 400-500 nm wavelength range indicates that even in the blend films, the supramolecular interaction of fullerenes with TPC is happening. Another prominent observation is the blue shift of overall absorption in the longer wavelength region (750-800 nm) of the blend films. Since this band edge mainly corresponds to the donor PTB7 molecules, and no such shift has been observed for neat PTB7 added with TPC, this indicates that in blend films, introduction of TPC causes the reduced inter-chain interaction between the PTB7 molecules in PTB7:$PC_{61}BM$:TPC blends compared to PTB7:$PC_{61}BM$.[45-46] The steric bulk of the TPC molecule can disrupt the π-π stacking and increase the spatial separation of the polymer backbone.[44] The reduced intensity of the π-π*(0,0) absorption peak corresponding to PTB7 molecules at ~ 670 nm further supports the reduced intermolecular interaction between the donor molecules in the blend film added with TPC.

The obtained increase in open circuit voltage also agrees with the observed blue shift of the PTB7:$PC_{61}BM$ blend films with TPC added (~40 meV) in their absorption spectra. The enhanced V_{oc} can thus be correlated to the reduced intermolecular interaction between

donor/acceptor molecules in the PTB7:PC_{61}BM blend film containing TPC and hence the lowered exciton binding energy for the photogenerated excitons. To confirm the contribution of lowered exciton binding energy, and hence a higher CT state energy, electroluminescence (EL) spectra of the PTB7:PC_{61}BM and PTB7:PC_{61}BM: TPC solar cells were measured and analysed.

The electroluminescence spectra of the PTB7:PC_{61}BM and PTB7:PC_{61}BM:TPC devices as a function of applied voltage is given in **Figure 5**. In both cases the CT state emission intensity systematically increases with increase in applied bias. In the case of PTB7:PC_{61}BM blend, the EL emission peak is centred around 885 nm corresponding to a CT state energy of 1.394 eV. However, for the case of TPC:PTB7:PC_{61}BM devices, the EL emission peak is centred at 864.5 nm and corresponds to a CT state energy of ~1.434 eV. The higher CT energy by an amount of ~ 40 meV is closely matching with the improved V_{oc} observed from the respective solar cell devices. The higher CT state energy would reduce the energetic loss between E^{*}_{D}-E_{CT} and E_{CT}-E_{A}^{*} and can thus account for the increased V_{oc}, where E^{*}_{D} and E_{A}^{*} are singlet excited states of donor and acceptor molecules respectively.[47] In the EL spectrum of PTB7:PC_{61}BM devices, at high applied biases, a shoulder peak starts to emerge at around 780 nm and it matches with the singlet exciton emission from the PTB7 donor molecules previously reported by Hedley et al.[34] This implies that some electrons in the CT state gain enough energy at high bias to flow over to the energy barrier and transfer to the PTB7. However, this emission peak is absent from the PTB7:PC_{61}BM added with TPC and this can be due to the faster dissociation of the CT complex because of low binding energy (corresponding to high CT state energy).
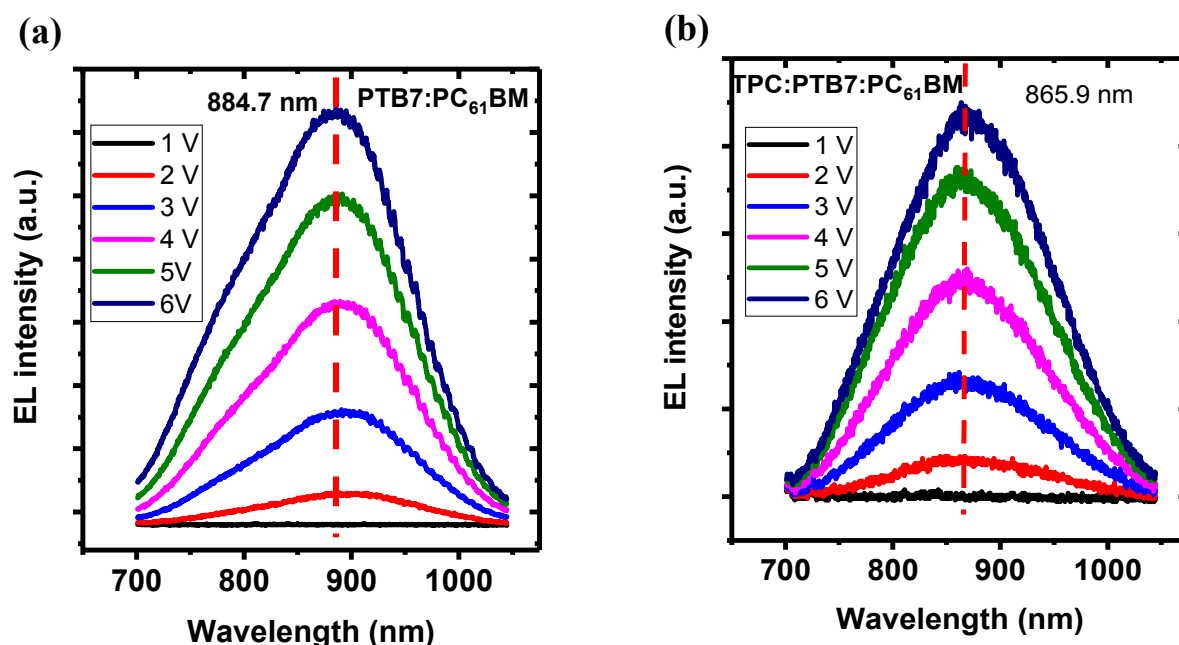
Figure 5. Electroluminescence spectra of the (a) PTB7-PC$_{61}$BM and (b) TPC:PTB7:PC$_{61}$BM blend based OPV devices.

The factors affecting the charge transfer state energy are electrochemical oxidation and reduction potentials of the donor and acceptor, Coulomb binding energy between the positive and negative charge, and polarization effects. Apart from these factors, CT state delocalization due to donor or acceptor aggregation has been shown to reduce the E$_{CT}$.[47-48] Surface morphology images by AFM (discussed in section 2.5(a)) show that neat blends of PTB7:PC$_{61}$BM has a coarse phase separated morphology which gets finer when TPC additive is mixed to PTB7:PC$_{61}$BM blend. The aggregated fullerenes can reduce the CT state energy (hence the redshifted EL emission peak for neat PTB7:PC$_{61}$BM blend).[49] The presence of TPC prevents the

aggregation of fullerene molecules by supramolecular self-assembly and also reduces the PTB7 inter-chain interaction as shown by the absorption spectra in Figure 4. These factors would decrease the CT state delocalization compared to films without TPC, increasing the E_{CT}.

To measure any effect of TPC on the energetic levels of donor and acceptor molecules, cyclic and square wave voltammetry (CV and SWV) studies were conducted for TPC, and air photoemission spectra (APS) were recorded for neat and TPC-containing donor and acceptor thin films, as described in the following section. The HOMO and LUMO levels of the TPC estimated from the density functional theory (DFT) calculations are -5.9 eV and -0.14 eV respectively. The CV and SWV traces of the TPC molecule are given in **Figure S9**. However, the traces are largely featureless in the potential window investigated, making it difficult to estimate values of the electron affinity (EA) and ionisation potential (IP) of TPC. TPC is electronically very similar to benzene as the three rings are not conjugated with each other, so it is unlikely that TPC is playing a direct role in the blend electronic structure. APS spectra (photoemission yield vs incident UV photon energy) of the neat PTB7 and PTB7 thin films containing TPC are given in **Figure S10 (a)**. Even though a slight blue shift (~15 meV) in the HOMO onset of PTB7 due to TPC incorporation is apparent, this is within the measurement error limit of the APS instrument: any energetic shift in the HOMO level of PTB7 with addition of TPC is below measurement threshold. Similarly, in the case of $PC_{61}BM$ (**Figure S10(b))**, TPC incorporation does not bring about any change in the HOMO level as seen by the consistency of the onset of photoemission yield for both neat and TPC modified molecules.

To investigate the effect of TPC on the electrochemical reduction potential (EA) of $PC_{61}BM$ and $PC_{71}BM$, thin films of these molecules with and without TPC were prepared in the identical conditions to those used for the solar cell device fabrication. **Figure S11 (a) and (b)**

shows the corresponding square-wave voltammogram plots. For the TPC containing $PC_{61}BM$ films, the SWV are significantly altered and displayed a shift in EA of ~ 80 mV. This shift in EA indicates that there is an interaction between the TPC and fullerene and that TPC is not merely a filler but interacts electronically with the fullerene. This shift in PCBM EA explains the origin of the higher CT state energy observed from the electroluminescence studies (in Figure 5) of the TPC containing $PTB7:PC_{61}BM$. For $PC_{71}BM$ the change in EA (~ 350 mV) is much larger than the change in V_{oc} (~ 40 mV). The type of negative shift observed in the first reduction wave of fullerene molecules implies that π-stacking of TPC and fullerene occurs in the films.[50-51] This difference in EA shift observed in $PC_{71}BM$ and $PC_{61}BM$ due to TPC incorporation further confirms different supramolecular interaction occurs within the film due to the differing sizes/shapes of the fullerene molecules. Previous complexation studies of C_{60} and C_{70} fullerene molecules by triptycene-derived calix[6]arenes using fluorescence titration studies have shown different binding energy values for complexation depending on the type of fullerene.[44, 52] This difference in binding energy for different fullerene molecules can support the observed difference in EA shift of $PC_{61}BM$ and $PC_{71}BM$ with TPC incorporation. However it should be noted that, compared to the EA shifts in $PC_{61}BM$ and $PC_{71}BM$ films (80 and 350 meV) with TPC added, the observed CT state energy shift (hence the V_{oc} ~ 40 meV) is smaller for PTB7:PCBM blends containing TPC, and this could be related to the different molecular arrangement and interface interactions between the donor and acceptor molecules in the blend compared to the neat film. This non-tracking behaviour of E_{CT} and V_{oc} on energy level shifts (HOMO donor and LUMO acceptor) has been recently reported for $RRa-P3HT:PC_{61}BM$ blend films.[53] The non-tracking behaviour was attributed to the presence of low energy band tails of CT density of states (under 1 Sun intensity with 10^{16} cm^{-3} charges only tail states are occupied) which sets the V_{oc}

and E_{CT} whereas in CV measurements, the donor HOMO-acceptor LUMO gap is determined by the centre of the density of states with no direct information about low-energy tails.[53] To substantiate this shift of EA in fullerene molecules due to TPC incorporation, P3HT:PCBM and PBDB-T:PCBM based solar cells were fabricated to investigate how the increased reduction potential affects the solar cell performance [**Figure S12(a) & (b), Figure S13 (a) & (b), Table S6**, **Table S7, and Table S8**]. P3HT and PBDB-T were selected as the donors since these molecules have much higher LUMO of ~ 3.0 eV and 2.92 eV compared to the fullerene molecules for which the LUMO is ~ 4 eV. Improved photovoltaic performance and hence increased power conversion efficiency due to enhanced FF and V_{oc} were observed in the case of both blends. The detailed discussion is included in SI.

To understand how the TPC incorporation is affecting the charge transport properties of the PTB7:PC$_{61}$BM blend films, electron and hole mobility is measured using space charge limited current measurements [**Figure S14**]. With the addition of TPC, the electron mobility of the PTB7:PC$_{61}$BM blend increases from $(1.23\pm0.12) \times 10^{-3}$ cm^{2}V^{-1}s^{-1} to $(2.54\pm0.29) \times 10^{-3}$ cm^{2}V^{-1}s^{-1}. The hole mobility does not change within the error bars; without TPC, the hole mobility is $(1.64\pm0.12) \times 10^{-3}$ cm^{2}V^{-1}s^{-1} and with TPC additive, hole mobility is $(1.78\pm0.31) \times 10^{-3}$ cm^{2}V^{-1}s^{-1}. This increased electron mobility by TPC clearly indicates that the fullerene connectivity and hence the percolative pathways to electrodes has been improved due to supramolecular interactions in the TPC:PTB7:PC$_{61}$BM blend.[33] Compared to the improvement in electron mobility, the hole mobility of PTB7:PC$_{61}$BM blend is not improved by TPC incorporation. This improved mobility of charge carriers upon TPC addition can account for the improved FF observed for the PTB7:PC$_{61}$BM blend solar cells added with TPC.

So far, the optoelectronic properties of the PTB7:PC$_{61}$BM blends with and without TPC addition have been discussed in detail. To investigate the microstructural and morphological properties of PTB7:PC$_{61}$BM blends influenced by adding TPC, Grazing Incidence Wide Angle X-ray Scattering (GIWAXS) and atomic force microscopy (AFM) measurements were carried out as discussed below.

2.5. Microstructural properties of PTB7:PC$_{61}$BM blends due to TPC addition

2.5 (a) Surface morphology by atomic force microscopy (AFM)

The surface topography and phase images of the PTB7-PC$_{61}$BM blend films with and without TPC were obtained by tapping mode atomic force microscopy. In the case of the neat PTB7:PC$_{61}$BM blend, the height and phase images are given in **Figure 6(a) and (b)**. From these images, large domains of fullerenes embedded in large regions of polymer matrix are clearly evident and the feature sizes range from ~100-300 nm. This kind of morphology with isolated large domains implies a lack of mutual solubility between the polymer and fullerene phases, leading to their aggregation. The AFM height and phase images for the PTB7:PC$_{61}$BM blend films with TPC added are given in **Figure 6(c) and (d)** respectively. Compared to neat PTB7-PC$_{61}$BM blends, in the case of blend films with TPC added, the domain size is dramatically reduced (less than 50 nm). This improved nano-scale morphology is beneficial for efficient exciton dissociation and can lead to an interpenetrated blending through percolating pathways. This is evidenced by increased charge carrier mobility and efficient charge collection reflected in higher FF of the PTB7:PC$_{61}$BM solar cells added with TPC. The difference in BHJ morphology for PTB7:PC$_{61}$BM blends with and without TPC implies that, the incorporation of TPC modifies the interaction between the donor and acceptor to promote supramolecular interactions and

increases the entropy of mixing of the two components.[54-55] It is worth noting that there is only a small change in the root mean square (RMS) roughness of the blend films; TPC incorporation slightly reduces the RMS roughness from 1.4 to 1.3 nm.
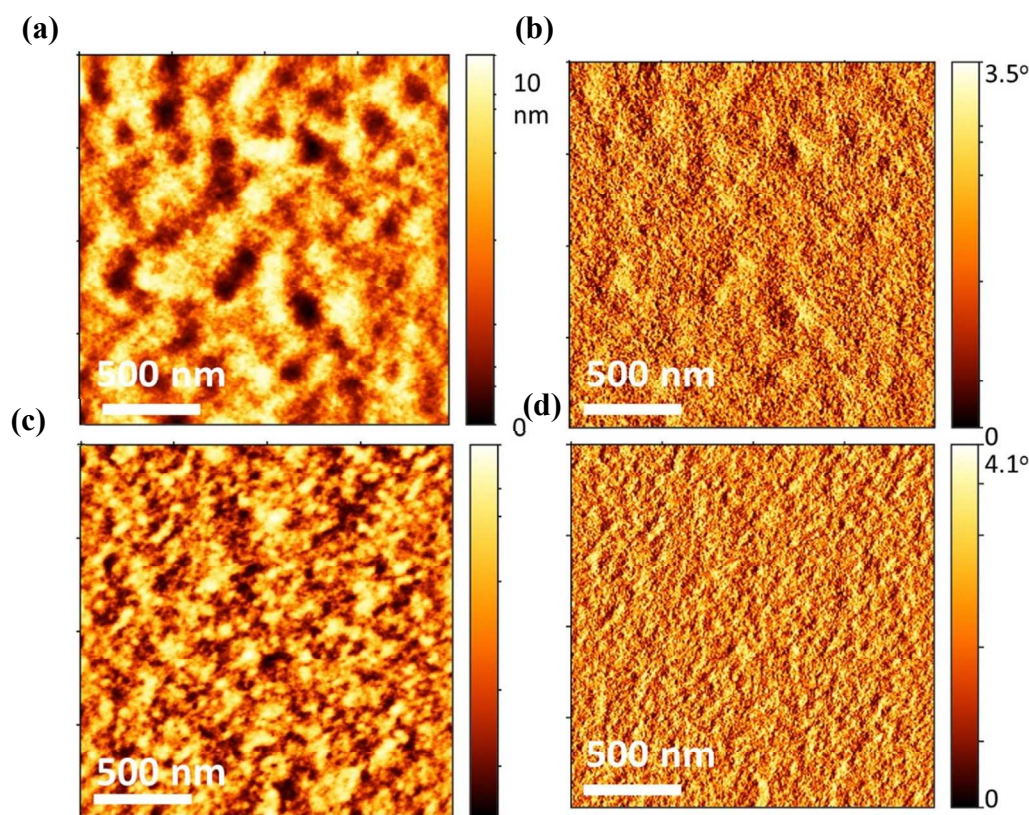

Figure 6. Atomic force microscopy height images for (a) PTB7:PC$_{61}$BM and (c) PTB7:PC$_{61}$BM blend films added with TPC. The corresponding phase images are shown in (b) and (d) respectively.

2.5 (b) Structural properties by GIWAXS analysis

To investigate how the structural properties of the PTB7:PC$_{61}$BM blend films are modified by TPC driven supramolecular interaction, GIWAXS measurements were carried out for blend films with and without added TPC (optimized conditions). The corresponding 2D-

GIWAXS patterns and integrated cake slices are shown in **Figure 7.** After applying necessary geometry corrections, we can identify three peaks typical of $PC_{61}BM$ (at $Q\approx0.7$, 1.36, and 1.96 $Å^{-1}$) and peaks associated with the polymer alkyl stacking peak ($Q=0.36$ $Å^{-1}$) and the polymer π-stacking peak ($Q=1.6$ $Å^{-1}$). The π-stacking peak appears as a shoulder which is mostly prominent in the out-of-plane direction, suggesting a face-on orientation. On the other hand, the alkyl peak appears isotropic, indicating that preferential face-on orientation is very weak. The appearance of similar features between the two images implies that there is no preferential orientation change introduced by the supramolecular interaction with TPC.

Overall, the addition of TPC results in subtle changes to the GIWAXS pattern and quantitative peak fitting was necessary to determine whether TPC affects the relative peak intensities. The peak intensities roughly correlate to the degree of crystallinity/aggregation of the corresponding components. Results from these fits are presented in Table S9. Adding TPC to the blend results in only small changes to the PTB7 and PCBM peak intensities which are within expected experimental error. Given the changes to domain segregation evident from AFM, this result is somewhat surprising. It shows that while domain sizes decrease with TPC inclusion, the composition of the domains remains constant.

When TPC is added, the alkyl peak position moves from 0.41 to 0.39 $Å^{-1}$, indicating an increase in alkyl stacking distance (from 15.3 to 16.1 Å). This increased alkyl spacing is in good agreement with the observed UV-vis absorption spectra, where reduced inter-chain interaction is observed for the $PTB7:PC_{61}BM$ blend with TPC additive. While it is difficult to determine the cause, this result shows that TPC has a significant effect on the local environment of PTB7. Meanwhile, the most intense (2nd) PCBM peak appears to move to higher Q with the addition of TPC, but this may be an artefact from overlap with the π-stacking peak of PTB7. Hence

GIWAXS data was collected for neat $PC_{61}BM$ films with and without TPC. Both 2D images and the respective 1D plots are shown in **Figure S15.** This data definitively shows that $PC_{61}BM$ peak positions shift from 0.74 $Å^{-1}$ and 1.42 $Å^{-1}$ in the neat film to 0.75 $Å^{-1}$ and 1.46 $Å^{-1}$ in the film with TPC added, confirming the trend to larger Q (closer spacing of $PC_{61}BM$) in the $PTB7:PC_{61}BM$. The corresponding 1D integrated plots are shown in Figure S16. For both PTB7 and PCBM, peak widths slightly increase when TPC is added, showing a larger range of packing distances in both materials. Thus, both PTB7 and PCBM packing are influenced by the presence of TPC: PTB7 becomes farther packed in the alkyl direction and PCBM becomes closer packed, and both have a higher disorder in packing distance. It is important to note that these changes are all of low magnitude, and overall the incorporation of TPC molecules has little influence on the crystalline properties of the $PTB7:PC_{61}BM$ blend. The more dramatic changes to the nanoscale segregation are expected to dominate over these small effects.
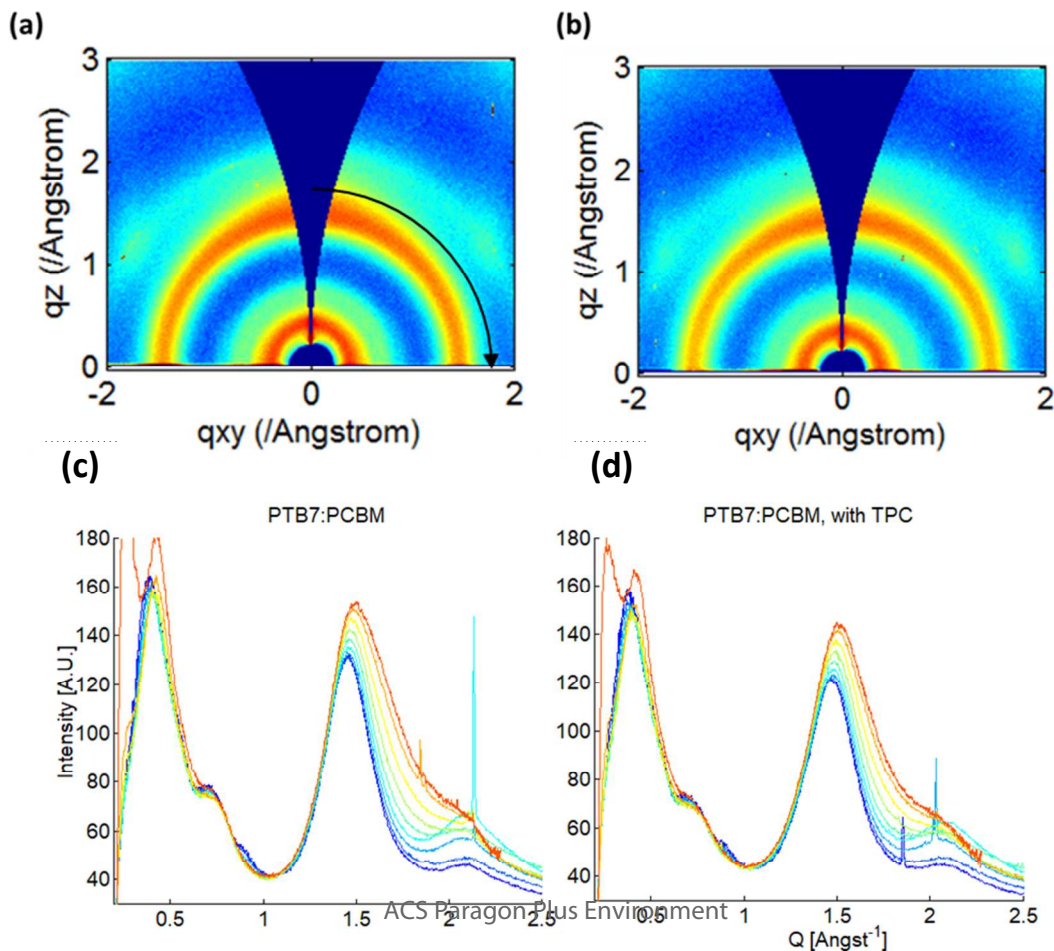
Figure 7: 2D-GIWAXS data of (a) PTB7:PC$_{61}$BM and (b) PTB7:PC$_{61}$BM blend added with TPC. (c) The corresponding integrated cake slices of PTB7:PC$_{61}$BM and (d) PTB7:PC$_{61}$BM blend with TPC. Each trace represents data from a 10° wedge in the images. Out-of-plane data (starting at 80-90°) is in red while in-plane data (at 0-10°) is in blue. Black arrows point from OOP to IP.

Thus based on the optoelectronic and microstructural characterization of PTB7:PC$_{61}$BM blend with and without TPC incorporation, we find the improved photovoltaic properties of the blend with added TPC are due to fine nanoscale segregation, the increase in CT state energy (lowering the driving force for electron transfer from donor to acceptor molecules) and enhanced electron mobility. These changes are all induced by the supramolecular interaction of TPC with both PTB7 and PC$_{61}$BM but fall short of a definite supramolecular templating or self-assembly of the domains since this type of interaction would imply higher degree of crystalinity in those domains. Having summarised the role of TPC in improving the photovoltaic properties of PTB7:PC$_{61}$BM blends, in the next section the optoelectronic and microstructural properties of PTB7:PC$_{71}$BM blend added with TPC are discussed.

2.6. Optoelectronic and Microstructural properties of PTB7:PC$_{71}$BM blends due to TPC addition

As demonstrated in session 2.2, similar to PTB7:PC$_{61}$BM blend, PTB7:PC$_{71}$BM blend has also shown an improved photovoltaic performance due to TPC addition. To correlate the observed photovoltaic properties of PTB7:PC$_{71}$BM with the photophysical and electronic

properties of the blend, UV-vis absorption spectra, air photoemission spectroscopy, square wave voltammetry and AFM imaging was carried out for neat and TPC added $PC_{71}BM$ and $PTB7:PC_{71}BM$ films. **Figure S17** shows the UV-vis absorption spectra of the $PC_{71}BM$ films and $PTB7:PC_{71}BM$ blend films with and without TPC. Unlike in $PC_{61}BM$, the TPC addition to $PC_{71}BM$ films doesn't change the absorption profile of $PC_{71}BM$, but an overall decrease in absorption is observed. This difference in optical absorption properties indicates that the supramolecular interaction effect due to TPC incorporation is different for $PC_{61}BM$ and $PC_{71}BM$. This could be related to the difference in symmetry between the two fullerene molecules as discussed by Williams *et al.*[40] In the blend films also, $PTB7:PC_{71}BM$ blend added with TPC shows a slightly lower absorbance in support of the absorbance spectra of neat and TPC added $PC_{71}BM$ films. The corresponding steady state photoluminescence spectra of the $PC_{71}BM$ and $PTB7:PC_{71}BM$ thin films with and without TPC additive are shown in **Figure S18.** Even though the effect is smaller than for $PC_{61}BM$ with TPC added, the PL emission spectra of $PC_{71}BM$ with TPC added also show a slight blue shift and narrowing of FWHM, suggesting the reduced intermolecular interaction between the $PC_{71}BM$ molecules due to TPC incorporation. However the effect is more clearly visible in the PL emission spectra of the blend films. A clear PL emission blue-shift and narrowing of the PL emission FWHM is observed for $PTB7:PC_{71}BM$ blend films added with TPC [Figure S18 (b)]. Air photoemission spectroscopy of the $PC_{71}BM$ films with and without TPC are shown in **Figure S19**. However no difference is observed for the onset energy for photoemission.

To investigate how supramolecular interactions with TPC is affecting the morphology of the $PTB7:PC_{71}BM$ blends, atomic force microscopy images were taken for both neat and TPC added blend films. The corresponding AFM height and phase images for the $PTB7:PC_{71}BM$ and

TPC:PTB7:PC_{71}BM blend films are shown in **Figure 8**. Similarly to PTB7:PC_{61}BM blends, addition of an optimized content of TPC reduces the domain size and nano-scale morphology of BHJ is obtained. In films of PTB7:PC_{71}BM without TPC the domain size is ~ 200-300 nm and the PC_{71}BM is highly aggregated in large domains. However with TPC added, the domain size is dramatically reduced to ~ 50-80 nm. This nanoscale morphology can enhance the exciton dissociation efficiency (as shown in Figure S4 (b)) and can explain the observed increase in Jsc and the corresponding improvement in EQE due to TPC incorporation to the PTB7:PC_{71}BM
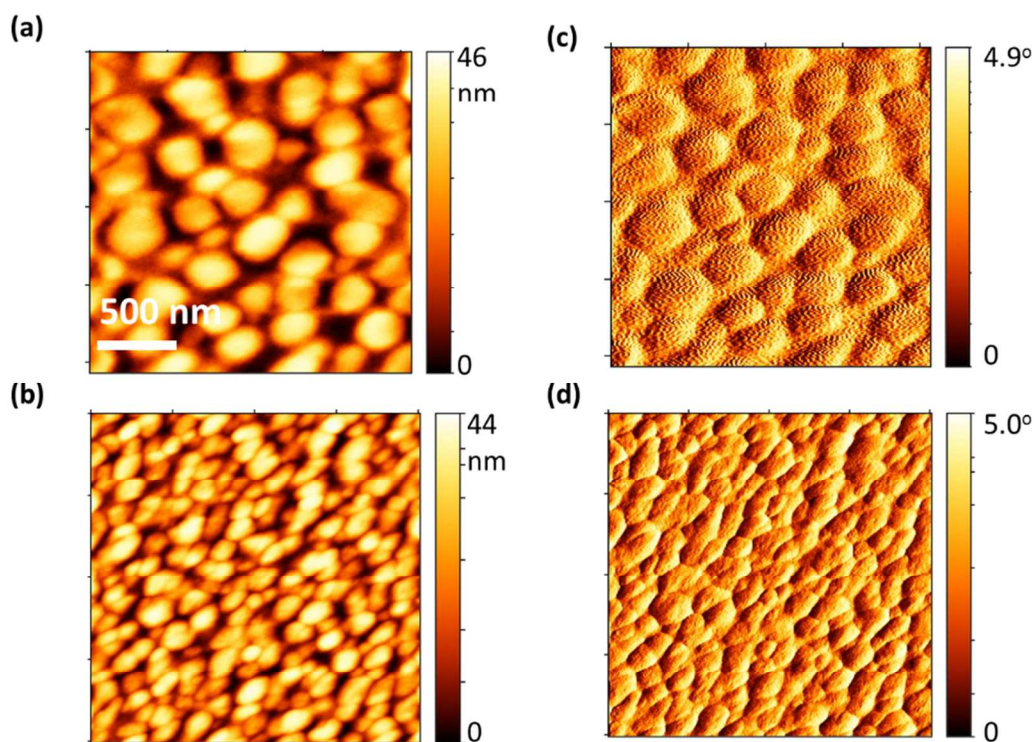
blend. The RMS roughness of the PTB7:PC_{71}BM and TPC:.PTB7:PC_{71}BM blend films are respectively 7.7 and 6.5 nm. Between the blend morphologies for PTB7:PC_{61}BM and PTB7:PC_{71}BM, **[(Figure 6(c) and (d)** *vs* **Figure 8 (c) and (d)]**, the finer morphology is obtained for the PTB7:PC_{61}BM:TPC blend, which can be due to the more spherical symmetry of the PC_{61}BM molecule.[28, 40]

Figure 8. Atomic force microscopy height images for (a) PTB7:PC$_{71}$BM and (b) PTB7:PC$_{71}$BM blend films added with TPC. The corresponding AFM phase images are shown in Figure 8(c) and (d).

To verify the contribution of CT state energy to the observed V_{oc} increase, electroluminescence spectra of the PTB7:PC$_{71}$BM solar cells with and without TPC were measured. **Figure S20** shows the EL spectra obtained as a function of different biasing conditions. In both blends of PTB7:PC$_{71}$BM with and without TPC, the CT state emission intensity systematically increases with increase in applied bias. In the case of PTB7:PC$_{71}$BM blend, the EL emission peak is centred around 887 nm corresponding to a CT state energy of 1.398 eV. However, for the case of TPC: PTB7:PC$_{71}$BM devices, the EL emission peak is centred at 859.3 nm and corresponds to a CT state energy of ~1.443 eV. The higher CT energy by an amount of ~45 meV is closely matching with the improved V_{oc} observed from the respective solar cell devices. Similar to the case of PTB7:PC$_{61}$BM blend, this higher CT state energy will reduce the driving force for E^{*}_{D}-E_{CT} and E_{CT}-E_{A}^{*}. Thus the difference in CT state energy observed for the PTB7:PC$_{71}$BM and PTB7:PC$_{61}$BM solar cells with TPC addition is comparable to the increased open circuit voltage.

It is worth noting that the improvement in J_{sc} of the solar cells for PTB7:PC$_{71}$BM with TPC added (33 %) is higher than that of the PTB7:PC$_{61}$BM blend with TPC added (5 %). This has been further confirmed by the respective EQE spectra shown in Figure 2 (c) and 3(c). Comparison of the absorption spectra [Figure 4(d) and Figure S18(b)] shows that this increase in EQE (hence in J_{sc}) is not due to an increase in absorption when TPC is added to the blends. Thus the origin of this improved Jsc can be related to the TPC induced different microstructural changes in the PTB7:PC$_{61}$BM and PTB7:PC$_{71}$BM blend, leading to differences in

photogeneration and charge collection properties. AFM images in Figure 6 and Figure 8 show a

finer surface topography for PTB7:PC$_{61}$BM blend with TPC added compared to the

PTB7:PC$_{71}$BM blend with TPC added. Though a finer length scale of phase separation favours

increased photogeneration of charges, the recombination probability is higher. However the

increased FF (by 50 %) for PTB7:PC$_{61}$BM with TPC added solar cells compared to the blend

without additive suggests that despite this finer morphology and trade off with higher probability

for recombination losses, the collection efficiency of photogenerated charges is improved. This

can be attributed to the closer packing of PC$_{61}$BM in PTB7:PC$_{61}$BM with added TPC (as shown

in GIWAXS studies) and the increased electron mobility as shown by SCLC measurements. In

the case of PTB7:PC$_{71}$BM with added TPC, the length scale of phase separation is slightly larger

(domain size of ~ 50-80 nm) compared to the PTB7:PC$_{61}$BM blend with added TPC (domain

size is less than 50 nm) and still retains a nano-scale morphology. This nanoscale morphology

enhances the exciton harvesting, and hence the photogeneration of charge carriers but is not so

fine as to increase recombination losses. This is supported by the increased photocurrent density

and the higher exciton dissociation probability for PTB7:PC$_{71}$BM blend with added TPC (shown

in Figure S4). Moreover the FF is also improved by ~ 16 % PTB7:PC$_{71}$BM blend with added

TPC compared to its neat blend.

2.7 Supramolecular modification of PTB7:PCBM blends by TPC additive

As explained in the introduction, TPC has been reported to lead to templating of

fullerenes.[26] These properties of self-assembly and supramolecular interaction of TPC have been

attributed to the high energy barrier of twisting/deformation giving it structural rigidity, the

internal free volume created by the three bladed geometry and the three aromatic phenyl rings

allowing TPC to have both electron rich and electron deficient rings in the same molecule.[43] The

supramolecular interaction of TPC with neat $PC_{61}BM$, neat $PC_{71}BM$ and the blends of

$PTB7:PC_{61}BM$, $PTB7:PC_{71}BM$ has been investigated by following the changes in the optical

absorption and fluorescence properties, shift in the LUMO energy level, structural packing and

surface morphology. UV-vis absorption spectra of neat and TPC added $PC_{61}BM$ and

$PTB7:PC_{61}BM$ blends showed a reduced intensity for the absorption in the wavelength range

(420-500 nm) corresponding to the dipole forbidden HOMO-LUMO transition in one $PC_{61}BM$ or

intermolecular HOMO-LUMO transition of adjacent $PC_{61}BM$ molecule. Further, in the

$PTB7:PC_{61}BM$ blend with TPC added, a blue shift in long wavelength absorption edge

corresponding to PTB7 is observed. These changes in the absorption properties imply that the

presence of TPC modifies the π- π stacking and local environment of PTB7 and/or $PC_{61}BM$

molecules confirming the supramolecular interaction of TPC in these domains. Now considering

the changes in energy level, Torrente *et al.*[41] have previously reported the effect of screening on

the energy level alignment of C_{60} molecules; the LUMO shifts between isolated C_{60} molecules,

C_{60} islands and C_{60} clusters. The observed upward LUMO shift (~80 meV) in $PC_{61}BM$ with

TPC added, and the evidence of higher CT state energy (~40 meV) in $PTB7:PC_{61}BM$ blend with

TPC added, suggests that TPC changes the molecular environment (hence the polarizability) of

$PC_{61}BM$ by supramolecular interaction and self-assembly process. The different amounts of

LUMO shift in $PC_{61}BM$ and $PTB7:PC_{61}BM$ blends are due to the different number of molecular

near neighbours in neat $PC_{61}BM$ and $PTB7:PC_{61}BM$ blends and the added interaction of TPC

with PTB7 which may minimise the interaction of TPC with $PC_{61}BM$ between neat and blended

films. Another aspect that supports the TPC induced supramolecular process is the optimized

molar ratio of $PC_{61}BM$ to TPC (1:2) for better photovoltaic properties, for which Chong *et al.*[43]

have previously reported a self-assembled close packed sheets of C_{60} separated by a layer of

TPC. This close packing has been supported by the differences in X-ray scattering from GIWAXS data of $PC_{61}BM$ films with and without TPC. Fluorescence quenching of TPC by $PC_{61}BM$ molecules indicates that a host-guest interaction can already take place before the spin-coating process itself. A much finer nanoscale morphology of the TPC incorporated PTB7:PCBM blends compared to the blend morphology without TPC also suggests that the presence of TPC promotes supramolecular interactions with the different components. The differences in absorption spectral features, upward shift in LUMO, different optimum ratio of fullerene : TPC to obtain best OPV performance in the case of $PC_{71}BM$ and for PTB7:$PC_{71}BM$ blend clearly points that TPC induced self-assembly by supramolecular interaction is largely affected by the size and symmetry of the fullerene molecule. However, as previously discussed the lack of overall gain in crystallinity in the polymer:fullerene domains falls short of a clear self-assembly or templating process in the film formation. Yet, the overwhelming influence of TPC on the morphology and optoelectronic properties in the blend films clearly supports the influence of supramolecular interactions on the improvement of photovoltaic properties.

So far the improved photovoltaic properties of the PTB7:$PC_{61}BM$ and PTB7:$PC_{71}BM$ blends added with TPC and reasons behind this enhancement have been discussed. In the next section the stability aspects of these OPVs are discussed.

2.8 Photostability of the PTB7:PCBM blends loaded with TPC

To test the photostability, representative solar cells were taken from both PTB7:$PC_{61}BM$ and PTB7:$PC_{71}BM$ with TPC, with DIO and without any additive. Initially, these solar cells were encapsulated using UV-cured epoxy inside a glove box and the PCE is monitored for ~ 35 hours of continuous irradiance of 1 Sun in air ambient. **Figure 9** shows the normalised PCE after

the photostability measurements for both PTB7:PC$_{71}$BM and PTB7:PC$_{61}$BM solar cell devices. Irrespective of the fullerene acceptor molecule, PTB7:PCBM blends added with DIO showed the highest drop in power conversion efficiency or least retention of photovoltaic power conversion efficiency (~55 % and 30 % for PTB7:PC$_{61}$BM and PTB7:PC$_{71}$BM blends respectively). The photoinduced instability of DIO added OPV blend systems has been recently investigated in detail and has been mainly attributed to the remnant iodine induced oxidation of fullerene molecules.[14-15] Compared to PTB7:PC$_{71}$BM (without any additive) blends, the PTB7:PC$_{61}$BM blend based solar cells showed better (~10% higher) photostability. The enhanced photochemical degradation and trap formation under photoirradiation for PTB7:PC$_{71}$BM blend has been previously reported by Koster et al.[56]

Now considering the photostability of PTB7:PCBM blends with TPC added, in both cases of fullerenes- PC$_{61}$BM and PC$_{71}$BM- the solar cells fabricated with TPC as additive showed better photostability compared to DIO as additive (~80% for PTB7:PC$_{61}$BM and ~70 % for PTB7:PC$_{71}$BM). In the case of the PTB7:PC$_{71}$BM, the blend with TPC added showed even better retention of photovoltaic properties compared to the neat blend and the blend with DIO added. In order to understand the better photostability of TPC added PTB7:PCBM solar cells, variation of individual photovoltaic performance parameters (J$_{sc}$, V$_{oc}$ and FF) as a function of light exposure time is analysed as shown in Figure S21. As seen from Figure S21, for both PTB7:PC$_{61}$BM and PTB7:PC$_{71}$BM, the main photovoltaic performance parameters that are being drastically affected by light irradiation for blends added with DIO are J$_{sc}$ and FF. As per the previous investigations this can be attributed to the morphological instability arising from enhanced photodegradation of the donor: acceptor blend or the aggregation of fullerene molecules in the presence of DIO and light.[15-17, 57] This photochemical degradation and

aggregation of fullerene molecules can adversely affect the photogeneration of charge carriers (by decreasing the donor:acceptor interface area) and cause a drop in charge collection efficiency due to increased recombination losses by forming traps and isolated larger domains. In the case of solar cells of PTB7:PCBM blends with TPC added, as seen from Figure S21, the FF and J_{sc} are much less influenced by photoirradiation, implying better morphological stability of the active layer blend under photoirradiation. The GIWAXS, UV-vis spectra and AFM imaging show that TPC has a significant effect on PTB7 and PCBM local environment and the addition of TPC influences the packing of PTB7 and PCBM in the PTB7:PCBM blends. In the presence of TPC, PCBM gets closer packed and PTB7 farther packed in the alkyl direction. Previously Durrant et al.[58] and McGehee et al.[59-60] have shown that, the molecular packing and arrangement determine the photochemical degradation of polymer:fullerene solar cells. Thus the changes in packing of PTB7:PCBM blends induced by TPC could be the reason for the enhanced retention of photovoltaic performance. Moreover, the closer packing of PCBM by TPC results in enhanced electron mobility (as demonstrated in section 2.4 by SCLC measurements) and can suppress the losses in collection efficiency of photogenerated charge carriers. This electron mobility enhancement by closer packing of PCBM is significant in photostability as Koster et al.[56] have shown that in the case of PTB7:PCBM blends the photoirradiation mainly degrades the electron transport compared to the hole transport.

It is worth mentioning that in the case of PTB7:PC$_{61}$BM solar cells with added TPC, though the solar cells have better photostability compared to DIO added PTB7:PC$_{61}$BM blends, it lags behind that of the neat blend. The exact mechanism for this observation is not clear at this moment, but it may relate to the reduced electron affinity of PC$_{61}$BM upon TPC addition.
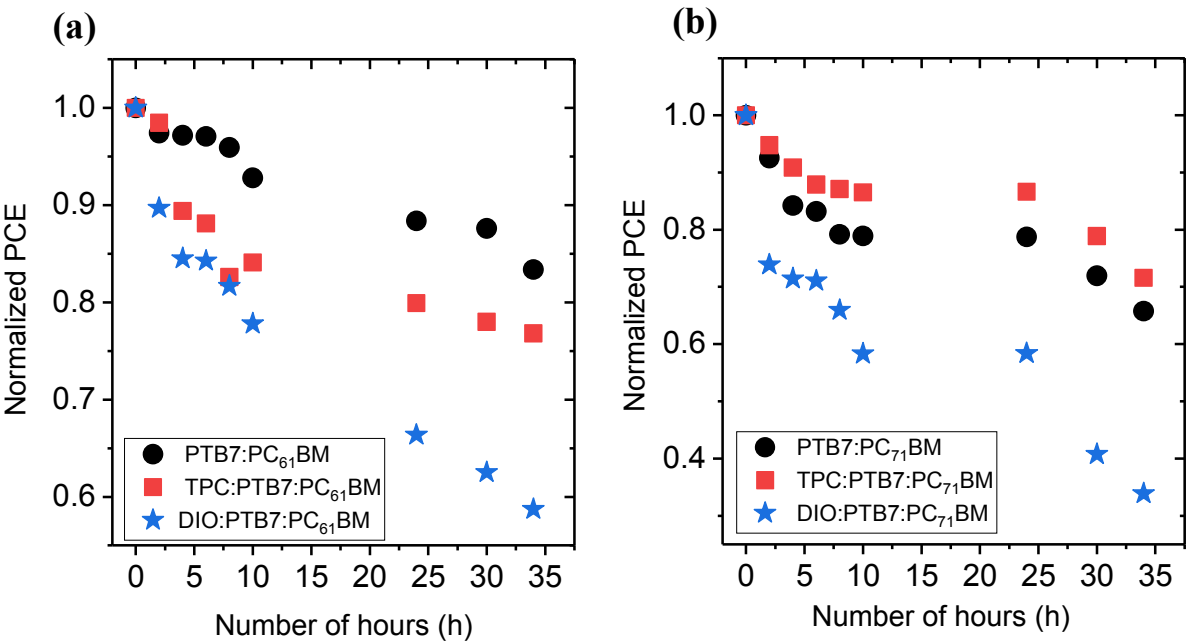
Figure 9: (a) Photostability comparison (for 1 Sun intensity) of the neat PTB7:PC$_{61}$BM blend

solar cells with that of DIO and TPC added blend (b) Photostability comparison of the neat

PTB7:PC$_{71}$BM blend solar cells with that of DIO and TPC added blend.

To investigate the thermal stability of the blends with TPC added, PTB7:PC$_{61}$BM blends with and without TPC (glass/ITO/a-ZnO/active layer blend) were thermally annealed (in N$_2$ ambient) at 130 ^{o}C for 30 minutes. Only a 7% drop in overall PCE is observed for PTB7:PC$_{61}$BM blends with TPC added. The respective J-V characteristics and the averaged (for 8 cells) solar cell performance parameters are shown in **Figure S22** and **Table S10**. Similar to the solar cells based on neat blend of PTB7:PC$_{61}$BM, the blend with added TPC also shows stable photovoltaic performance parameters especially for J$_{sc}$ and FF. In the previous studies where thermal annealing or photoirradiation interrupts the morphological stability, the photovoltaic performance parameters that have shown drastic drop in performance are FF and J$_{sc}$.[56-57, 61-62] However in the case of PTB7:PCBM blends with TPC added, under both photoirradiation (Figure S21) and thermal annealing (Figure S22 and Table S10), the FF and J$_{sc}$ are less affected indicating better morphological stability for the blends with TPC added.

Conclusion

The photovoltaic properties of the PTB7:PCBM blends upon TPC incorporation was investigated. The supramolecular interactions induced by the TPC additive beneficially modifies the absorption properties, CT state energy, molecular packing, donor/acceptor nanoscale phase separation and charge transport properties in the blend. Irrespective of the symmetry of the acceptor molecule, PC$_{61}$BM or PC$_{71}$BM, incorporation of TPC enhances the power conversion efficiency of the OPV devices. In contrast to previously reported additives such as DIO, where the enhancement in PCE has been mainly due to fine morphology-induced improvement in fill factor and higher photo-generation of charge carriers, TPC-induced PV performance parameters greatly depend upon the symmetry of the acceptor molecules as it drives the supramolecular interactions in the BHJ blend. Higher (~55% increase) fill factor enhancement has been obtained

when the acceptor molecule is more symmetrical ($PC_{61}BM$) compared to asymmetrical $PC_{71}BM$ acceptor (58% vs 42%). The substantial increase in open circuit voltage of ~ 40-50 meV, for both $PTB7:PC_{61}BM$ and $PTB7:PC_{71}BM$ blends upon TPC incorporation has been shown to be due to the increased CT state energy, which lowers the driving force for electron transfer. Similar improvement in efficiency (mainly by V_{oc} improvement) was demonstrated for other BHJs such as P3HT:PCBM and PBDB-T:PCBM blends. A comparison of the photostability measurements showed ~30% better retention of photovoltaic performance for PTB7:PCBM OPVs added with TPC compared to the respective devices with DIO as additive. Thus the present study highlights a simple method of using TPC as an additive for supramolecular modification of donor:acceptor components to form nanoscale phase separated morphology and to modify the energy levels to improve the photovoltaic properties of polymer solar cells. This property of TPC to modify the frontier orbitals and the morphology by using supramolecular interactions in the blend can be exploited in other optoelectronic devices such as organic light emitting diodes and organic photodetectors.

Conflicts of interest

There are no conflicts of interest to declare.

Acknowledgements

Supporting Information

The details of NMR spectra of TPC, table of photovoltaic performance parameters, SCLC measurement details, discussion on the effect of TPC on the photovoltaic properties of P3HT:PCBM and PBDB-T:PCBM blends

References

1. Zhao, W.; Li, S.; Zhang, S.; Liu, X.; Hou, J., Ternary Polymer Solar Cells based on Two Acceptors and One Donor for Achieving 12.2% Efficiency. *Adv. Mater.* **2017,** *29*, 1604059.

2. Zhao, W.; Qian, D.; Zhang, S.; Li, S.; Inganäs, O.; Gao, F.; Hou, J., Fullerene-Free Polymer Solar Cells with over 11% Efficiency and Excellent Thermal Stability. *Adv. Mater.* **2016,** *28*, 4734-4739.

3. Proctor, C. M.; Kuik, M.; Nguyen, T.-Q., Charge Carrier Recombination in Organic Solar Cells. *Prog. Polym. Sci.* **2013,** *38*, 1941-1960.

4. Long, Y.; Hedley, G. J.; Ruseckas, A.; Chowdhury, M.; Roland, T.; Serrano, L. A.; Cooke, G.; Samuel, I. D. W., Effect of Annealing on Exciton Diffusion in a High Performance Small Molecule Organic Photovoltaic Material. *ACS Appl. Mater. Interfaces* **2017,** *9*, 14945-14952.

5. Foertig, A.; Kniepert, J.; Gluecker, M.; Brenner, T.; Dyakonov, V.; Neher, D.; Deibel, C., Nongeminate and Geminate Recombination in PTB7:PCBM Solar Cells. *Adv. Funct. Mater.* **2014,** *24*, 1306-1311.

6. Kniepert, J.; Lange, I.; Heidbrink, J.; Kurpiers, J.; Brenner, T. J. K.; Koster, L. J. A.; Neher, D., Effect of Solvent Additive on Generation, Recombination, and Extraction in PTB7:PCBM Solar Cells: A Conclusive Experimental and Numerical Simulation Study. *J. Phys. Chem. C* **2015,** *119*, 8310-8320.

7. Verploegen, E.; Mondal, R.; Bettinger, C. J.; Sok, S.; Toney, M. F.; Bao, Z. A., Effects of Thermal Annealing Upon the Morphology of Polymer-Fullerene Blends. *Adv. Funct. Mater.* **2010,** *20*, 3519-3529.

8. Yi, Z.; Ni, W.; Zhang, Q.; Li, M.; Kan, B.; Wan, X.; Chen, Y., Effect of Thermal Annealing on Active Layer Morphology and Performance for Small Molecule Bulk Heterojunction Organic Solar Cells. *J. Mater. Chem. C* **2014,** *2*, 7247-7255.

9. Min, J.; Jiao, X. C.; Ata, I.; Osvet, A.; Ameri, T.; Bauerle, P.; Ade, H.; Brabec, C. J., Time-Dependent Morphology Evolution of Solution-Processed Small Molecule Solar Cells during Solvent Vapor Annealing. *Adv. Energy Mater.* **2016,** *6*, 1502579.

10. Huang, Y.-C.; Tsao, C.-S.; Cha, H.-C.; Chuang, C.-M.; Su, C.-J.; Jeng, U. S.; Chen, C.-Y., Correlation Between Hierarchical Structure and Processing Control of Large-area Spray-coated Polymer Solar Cells toward High Performance. *Sci. Rep.* **2016,** *6*, 20062.

11. Liao, H. C.; Ho, C. C.; Chang, C. Y.; Jao, M. H.; Darling, S. B.; Su, W. F., Additives for Morphology Control in High-Efficiency Organic Solar Cells. *Mater. Today* **2013,** *16*, 326-336.

12. Fu, P.; Guo, X.; Zhang, B.; Chen, T.; Qin, W.; Ye, Y.; Hou, J.; Zhang, J.; Li, C., Achieving 10.5% Efficiency for Inverted Polymer Solar Cells by Modifying the ZnO Cathode Interlayer with Phenols. *J. Mater. Chem. A* **2016,** *4*, 16824-16829.

13.   http://www.molbase.com/en/properties_24772-63-2-moldata-48193.html   (accessed 19/02/2018).

14.   Tremolet de Villers, B. J.; O'Hara, K. A.; Ostrowski, D. P.; Biddle, P. H.; Shaheen, S. E.; Chabinyc, M. L.; Olson, D. C.; Kopidakis, N., Removal of Residual Diiodooctane Improves Photostability of High-Performance Organic Solar Cell Polymers. *Chem. Mater.* **2016,** *28*, 876-884.

15.   Huang, W.; Gann, E.; Xu, Z.-Q.; Thomsen, L.; Cheng, Y.-B.; McNeill, C. R., A Facile Approach to Alleviate Photochemical Degradation in High Efficiency Polymer Solar Cells. *J. Mater. Chem. A* **2015,** *3*, 16313-16319.

16.   Lee, S.; Kong, J.; Lee, K., Air-Stable Organic Solar Cells Using an Iodine-Free Solvent Additive. *Adv. Energy Mater.* **2016,** *6*, 1600970.

17.   Jacobs, I. E.; Wang, F.; Bedolla Valdez, Z. I.; Ayala Oviedo, A. N.; Bilsky, D. J.; Moule, A. J., Photoinduced Degradation from Trace 1,8-diiodooctane in Organic Photovoltaics. *J. Mater. Chem. C* **2018,** *6*, 219-225.

18.   Cheng, P.; Yan, C.; Wu, Y.; Wang, J.; Qin, M.; An, Q.; Cao, J.; Huo, L.; Zhang, F.; Ding, L.; Sun, Y.; Ma, W.; Zhan, X., Alloy Acceptor: Superior Alternative to PCBM toward Efficient and Stable Organic Solar Cells. *Adv. Mater.* **2016**, *28*, 8021–8028.

19.   Chen, W.; Zhang, Q., Recent Progress in Non-fullerene Small Molecule Acceptors in Organic Solar Cells (OSCs). *J. Mater. Chem. C* **2017,** *5*, 1275-1302.

20.   Teng, Z.; Erik, B.; Joachim, L., Relating Morphological Characteristics to the Open-Circuit Voltage of Organic Bulk-heterojunction Solar Cells. *Appl. Phys. Express* **2015,** *8*, 024301.

21.   Elumalai, N. K.; Uddin, A., Open Circuit Voltage of Organic Solar Cells: an In-depth Review. *Energy Environ. Sci.* **2016,** *9*, 391-410.

22.   Chen, C.-F., Novel Triptycene-Derived Hosts: Synthesis and their Applications in Supramolecular Chemistry. *Chem. Commun.* **2011,** *47*, 1674-1688.

23.   Jiang, Y.; Chen, C.-F., Recent Developments in Synthesis and Applications of Triptycene and Pentiptycene Derivatives. *Eur. J. Org. Chem.* **2011,** *2011*, 6377-6403.

24.   Zhao, L. W.; Li, Z.; Wirth, T., Triptycene Derivatives: Synthesis and Applications. *Chem. Lett.* **2010,** *39*, 658-667.

25.   Swager, T. M., Iptycenes in the Design of High Performance Polymers. *Acc. Chem. Res.* **2008,** *41*, 1181-1189.

26.   Lomas, C. R.; Hodgkiss, J. M., Templated Growth of Fullerene C60 Crystals by Triptycene in Polymer Blend Films. *Supramol. Chem.* **2012,** *24*, 526-531.

27.   Konarev, D. V.; Drichko, N. V.; Lyubovskaya, R. N.; Shul'ga, Y. M.; Litvinov, A. L.; Semkin, V. N.; Dubitsky, Y. A.; Zaopo, A., Donor–Acceptor Interaction of Fullerene C60 with Triptycene in Molecular Complex TPC·C60. *J. Mol. Struct.* **2000,** *526*, 25-29.

28.   Marc Veen, E.; L. Feringa, B.; M. Postma, P.; T. Jonkman, H.; L. Spek, A., Solid state Organisation of C60 by Inclusion Crystallisation with Triptycenes. *Chem. Commun.* **1999,** 1709-1710.

29.   Jagadamma, L. K.; Abdelsamie, M.; El Labban, A.; Aresu, E.; Ngongang Ndjawa, G. O.; Anjum, D. H.; Cha, D.; Beaujuge, P. M.; Amassian, A., Efficient Inverted Bulk-Heterojunction Solar Cells from Low-Temperature Processing of Amorphous ZnO Buffer Layers. *J. Mater. Chem. A* **2014,** *2*, 13321-13331.

30.   Ilavsky, J., Nika: Software for Two-Dimensional Data Reduction. *J. Appl. Crystallogr.* **2012,** *45*, 324-328.

31. Oosterhout, S. D.; Savikhin, V.; Zhang, J.; Zhang, Y.; Burgers, M. A.; Marder, S. R.; Bazan, G. C.; Toney, M. F., Mixing Behavior in Small Molecule:Fullerene Organic Photovoltaics. *Chem. Mater.* **2017,** *29*, 3062-3069.

32. Frisch, M. J.; Trucks, G. W.; Schlegel, H. B.; Scuseria, G. E.; Robb, M. A.; Cheeseman, J. R.; Scalmani, G.; Barone, V.; Petersson, G. A.; Nakatsuji, H.; Li, X.; Caricato, M.; Marenich, A. V.; Bloino, J.; Janesko, B. G.; Gomperts, R.; Mennucci, B.; Hratchian, H. P.; Ortiz, J. V.; Izmaylov, A. F.; Sonnenberg, J. L.; Williams; Ding, F.; Lipparini, F.; Egidi, F.; Goings, J.; Peng, B.; Petrone, A.; Henderson, T.; Ranasinghe, D.; Zakrzewski, V. G.; Gao, J.; Rega, N.; Zheng, G.; Liang, W.; Hada, M.; Ehara, M.; Toyota, K.; Fukuda, R.; Hasegawa, J.; Ishida, M.; Nakajima, T.; Honda, Y.; Kitao, O.; Nakai, H.; Vreven, T.; Throssell, K.; Montgomery Jr., J. A.; Peralta, J. E.; Ogliaro, F.; Bearpark, M. J.; Heyd, J. J.; Brothers, E. N.; Kudin, K. N.; Staroverov, V. N.; Keith, T. A.; Kobayashi, R.; Normand, J.; Raghavachari, K.; Rendell, A. P.; Burant, J. C.; Iyengar, S. S.; Tomasi, J.; Cossi, M.; Millam, J. M.; Klene, M.; Adamo, C.; Cammi, R.; Ochterski, J. W.; Martin, R. L.; Morokuma, K.; Farkas, O.; Foresman, J. B.; Fox, D. J. *Gaussian 16*, Wallingford, CT, 2016.

33. Foster, S.; Deledalle, F.; Mitani, A.; Kimura, T.; Kim, K.-B.; Okachi, T.; Kirchartz, T.; Oguma, J.; Miyake, K.; Durrant, J. R.; Doi, S.; Nelson, J., Electron Collection as a Limit to Polymer:PCBM Solar Cell Efficiency: Effect of Blend Microstructure on Carrier Mobility and Device Performance in PTB7:PCBM. *Adv. Energy Mater.* **2014,** *4*, 1400311.

34. Hedley, G. J.; Ward, A. J.; Alekseev, A.; Howells, C. T.; Martins, E. R.; Serrano, L. A.; Cooke, G.; Ruseckas, A.; Samuel, I. D. W., Determining the Optimum Morphology in High-Performance Polymer-Fullerene Organic Photovoltaic Cells. *Nat. Commun.* **2013,** *4*, 2867.

35. Pranculis, V.; Ruseckas, A.; Vithanage, D. A.; Hedley, G. J.; Samuel, I. D. W.; Gulbinas, V., Influence of Blend Ratio and Processing Additive on Free Carrier Yield and Mobility in PTB7:PC$_{71}$BM Photovoltaic Solar Cells. *J. Phys. Chem. C* **2016,** *120*, 9588-9594.

36. Kumano, M.; Ide, M.; Seiki, N.; Shoji, Y.; Fukushima, T.; Saeki, A., A Ternary Blend of a Polymer, Fullerene, and Insulating Self-Assembling Triptycene Molecules for Organic Photovolatics. *J. Mater. Chem. A* **2016,** *4*, 18490-18498.

37. Lobez, J. M.; Andrew, T. L.; Bulović, V.; Swager, T. M., Improving the Performance of P3HT–Fullerene Solar Cells with Side-Chain-Functionalized Poly(thiophene) Additives: A New Paradigm for Polymer Design. *ACS Nano* **2012,** *6*, 3044-3056.

38. Zhao, L.; Zhao, S.; Xu, Z.; Qiao, B.; Huang, D.; Xu, X., Two effects of 1,8-diiodooctane on PTB7-Th:PC$_{71}$BM Polymer Solar Cells. *Org. Electron.* **2016,** *34*, 188-192.

39. Huang, D.; Li, Y.; Xu, Z.; Zhao, S.; Zhao, L.; Zhao, J., Enhanced Performance and Morphological Evolution of PTB7:PC71BM polymer solar cells by Using Solvent Mixtures with Different Additives. *Phys. Chem. Chem. Phys.* **2015,** *17*, 8053-8060.

40. Williams, M.; Tummala, N. R.; Aziz, S. G.; Risko, C.; Brédas, J.-L., Influence of Molecular Shape on Solid-State Packing in Disordered PC$_{61}$BM and PC$_{71}$BM Fullerenes. *J. Phys. Chem. Lett.* **2014,** *5*, 3427-3433.

41. Isabel Fernández, T.; Katharina, J. F.; Jose Ignacio, P., Spectroscopy of C 60 Single Molecules: the Role of Screening on Energy Level Alignment. *J. Phys. Condens. Matter* **2008,** *20*, 184001.

42. Orlandi, G.; Negri, F., Electronic States and Transitions in C60 and C70 Fullerenes. *Photochem. Photobiol. Sci.* **2002,** *1*, 289-308.

43. Chong, J. H.; MacLachlan, M. J., Iptycenes in Supramolecular and Materials Chemistry. *Chem. Soc. Rev.* **2009,** *38*, 3301-3315.

44. Mondal, S.; Chakraborty, S.; Bhowmick, S.; Das, N., Synthesis of Triptycene-Based Organosoluble, Thermally Stable, and Fluorescent Polymers: Efficient Host–Guest Complexation with Fullerene. *Macromolecules* **2013,** *46*, 6824-6831.

45. Dang, M. T.; Hirsch, L.; Wantz, G.; Wuest, J. D., Controlling the Morphology and Performance of Bulk Heterojunctions in Solar Cells. Lessons Learned from the Benchmark Poly(3-hexylthiophene):[6,6]-Phenyl-C61-butyric Acid Methyl Ester System. *Chem. Rev.* **2013,** *113*, 3734-3765.

46. Leblebici, S. Y.; Chen, T. L.; Olalde-Velasco, P.; Yang, W.; Ma, B., Reducing Exciton Binding Energy by Increasing Thin Film Permittivity: An Effective Approach To Enhance Exciton Separation Efficiency in Organic Solar Cells. *ACS Appl. Mater. Interfaces* **2013,** *5*, 10105-10110.

47. Vandewal, K., Interfacial Charge Transfer States in Condensed Phase Systems. *Annu. Rev. Phys. Chem.* **2016,** *67*, 113-133.

48. Koen, V.; Abay, G.; D., O. W.; Sabine, B.; Fateme, B.; Ineke, V. S.; Laurence, L.; J., C. T.; Dirk, V.; V., M. J., The Relation Between Open☐Circuit Voltage and the Onset of Photocurrent Generation by Charge☐Transfer Absorption in Polymer∶Fullerene Bulk Heterojunction Solar Cells. *Adv. Funct. Mater.* **2008,** *18*, 2064-2070.

49. Lin, Y.; Fusella, M.; Barry., R. The Impact of Local Morphology on Organic Donor/Acceptor Charge Transfer States. *Adv. Energy Mater.* **2018,** 1702816.

50. Nandwana, V.; Samuel, I.; Cooke, G.; Rotello, V. M., Aromatic Stacking Interactions in Flavin Model Systems. *Acc. Chem. Res.* **2013,** *46*, 1000-1009.

51. Breinlinger, E. C.; Rotello, V. M., Model Systems for Flavoenzyme Activity. Modulation of Flavin Redox Potentials through π-Stacking Interactions. *J. Am. Chem. Soc.* **1997,** *119*, 1165-1166.

52. Tian, X.-H.; Chen, C.-F., Triptycene-Derived Calix[6]arenes: Synthesis, Structures, and Their Complexation with Fullerenes C60 and C70. *Chem. Eur. J.* **2010,** *16*, 8072-8079.

53. Sweetnam, S.; Prasanna, R.; Burke, T. M.; Bartelt, J. A.; McGehee, M. D., How the Energetic Landscape in the Mixed Phase of Organic Bulk Heterojunction Solar Cells Evolves with Fullerene Content. *J. Phys. Chem. C* **2016,** *120*, 6427-6434.

54. Bronstein, H.; Leem, D. S.; Hamilton, R.; Woebkenberg, P.; King, S.; Zhang, W.; Ashraf, R. S.; Heeney, M.; Anthopoulos, T. D.; Mello, J. d.; McCulloch, I., Indacenodithiophene-co-benzothiadiazole Copolymers for High Performance Solar Cells or Transistors via Alkyl Chain Optimization. *Macromolecules* **2011,** *44*, 6649-6652.

55. Liu, Y.; Tang, D.; Zhang, K.; Huang, P.; Wang, Z.; Zhu, K.; Li, Z.; Yuan, L.; Fan, J.; Zhou, Y.; Song, B., Tuning Surface Energy of Conjugated Polymers via Fluorine Substitution of Side Alkyl Chains: Influence on Phase Separation of Thin Films and Performance of Polymer Solar Cells. *ACS Omega* **2017,** *2*, 2489-2498.

56. Bartesaghi, D.; Ye, G.; Chiechi, R. C.; Koster, L. J. A., Compatibility of PTB7 and [70]PCBM as a Key Factor for the Stability of PTB7:[70]PCBM Solar Cells. *Adv. Energy Mater.* **2016,** *6*, 1502338.

57. Krishnan Jagadamma, L.; Sajjad, M. T.; Savikhin, V.; Toney, M. F.; Samuel, I. D. W., Correlating Photovoltaic Properties of a PTB7-Th:PC71BM Blend to Photophysics and

Microstructure as a Function of Thermal Annealing. *J. Mater. Chem. A* **2017,** *5*, 14646-14657.

58.   W., S. Y.; Safa, S.; Shahid, A. R.; Hugo, B.; C., S. B.; Weimin, Z.; Zhuping, F.; Martin, H.; Iain, M.; R., D. J., Material Crystallinity as a Determinant of Triplet Dynamics and Oxygen Quenching in Donor Polymers for Organic Photovoltaic Devices. *Adv. Funct. Mater.* **2014,** *24*, 1474-1482.

59.   Mateker, W. R.; Heumueller, T.; Cheacharoen, R.; Sachs-Quintana, I. T.; McGehee, M. D.; Warnan, J.; Beaujuge, P. M.; Liu, X.; Bazan, G. C., Molecular Packing and Arrangement Govern the Photo-Oxidative Stability of Organic Photovoltaic Materials. *Chem. Mater.* **2015,** *27*, 6345-6353.

60.   Cheacharoen, R.; Mateker, W. R.; Zhang, Q.; Kan, B.; Sarkisian, D.; Liu, X.; Love, J. A.; Wan, X.; Chen, Y.; Nguyen, T.-Q.; Bazan, G. C.; McGehee, M. D., Assessing the Stability of High Performance Solution Processed Small Molecule Solar Cells. *Sol. Energy Mater. Sol. Cells* **2017,** *161*, 368-376.

61.   Hsieh, Y.-J.; Huang, Y.-C.; Liu, W.-S.; Su, Y.-A.; Tsao, C.-S.; Rwei, S.-P.; Wang, L., Insights into the Morphological Instability of Bulk Heterojunction PTB7-Th/PCBM Solar Cells upon High-Temperature Aging. *ACS Appl. Mater. Interfaces* **2017,** *9*, 14808-14816.

62.   J., S. C.; M., P. C.; A., N. M.; Christian, B.; Gonzalo, S.; V., R. S.; Peter, M. B., Morphological Degradation in Low Bandgap Polymer Solar Cells – An In Operando Study. *Adv. Energy Mater.* **2016,** *6*, 1600712.

Table of Contents (TOC)